

Lawrence Berkeley National Laboratory

LBL Publications

Title

Quantifying the Uncertainties of Reanalyzed Arctic Cloud and Radiation Properties Using Satellite Surface Observations

Permalink

<https://escholarship.org/uc/item/9kx1p2zv>

Journal

Journal of Climate, 30(19)

ISSN

0894-8755

Authors

Huang, Yiyi
Dong, Xiquan
Xi, Baike
[et al.](#)

Publication Date

2017-10-01

DOI

10.1175/jcli-d-16-0722.1

Peer reviewed

Quantifying the Uncertainties of Reanalyzed Arctic Cloud and Radiation Properties Using Satellite Surface Observations

YIYI HUANG AND XIQUAN DONG

Department of Hydrology and Atmospheric Sciences, The University of Arizona, Tucson, Arizona

BAIKE XI,^a ERICA K. DOLINAR, AND RYAN E. STANFIELD

Department of Atmospheric Sciences, University of North Dakota, Grand Forks, North Dakota

SHAORYUE QIU

Department of Hydrology and Atmospheric Sciences, The University of Arizona, Tucson, Arizona

^a Current affiliation: Department of Hydrology and Atmospheric Sciences, The University of Arizona, Tucson, Arizona.

Corresponding author: Dr. Xiquan Dong, xdong@email.arizona.edu

Abstract

Reanalyses have proven to be convenient tools for studying the Arctic climate system, but their uncertainties should first be identified. In this study, five reanalyses (JRA-55, 20CRv2c, CFSR, ERA-Interim, and MERRA-2) are compared with NASA CERES-MODIS (CM)-derived cloud fractions (CFs), cloud water paths (CWPs), top-of-atmosphere (TOA) and surface longwave (LW) and shortwave (SW) radiative fluxes over the Arctic (70°–90°N) over the period of 2000–12, and *CloudSat-CALIPSO* (CC)-derived CFs from 2006 to 2010. The monthly mean CFs in all reanalyses except JRA-55 are close to or slightly higher than the CC-derived CFs from May to September. However, wintertime CF cannot be confidently evaluated until instrument simulators are implemented in reanalysis products. The comparison between CM and CC CFs indicates that CM-derived CFs are reliable in summer but not in winter. Although the reanalysis CWPs follow the general seasonal variations of CM CWPs, their annual means are only half or even less than the CM-retrieved CWPs (126 g m⁻²). The annual mean differences in TOA and surface SW and LW fluxes between CERES EBAF and reanalyses are less than 6 W m⁻² for TOA radiative fluxes and 16 W m⁻² for surface radiative fluxes. All reanalyses show positive biases along the northern and eastern coasts of Greenland as a result of model elevation biases or possible CM clear-sky retrieval issues. The correlations between the reanalyses and CERES satellite retrievals indicate that all five reanalyses estimate radiative fluxes better than cloud properties, and MERRA-2 and JRA-55 exhibit comparatively higher correlations for Arctic cloud and radiation properties.

Keywords: Arctic; Cloud cover; Cloud radiative effects; Radiative fluxes; Model comparison; Model evaluation/performance

1. Introduction

Previous studies have demonstrated that the Arctic is a region of importance and vulnerability to global climate change (IPCC 2013). To better predict long-term Arctic climate change, it is important to understand cloud and radiation processes, their interrelationships with atmospheric dynamics and the underlying boundary, and their impacts on the Arctic climate system (Curry et al. 1996). Generally, clouds impact the shortwave (SW) radiation budget primarily through their high albedo and have an impact on longwave (LW) radiation by changing atmospheric emissivity and emitting temperature (Gorodetskaya and Tremblay 2008). However, because of the high albedo of the snow/ice surface, large solar zenith angle, the absence of solar radiation during winter, extremely low temperatures and humidity, the presence of temperature inversions, and the frequent occurrence of supercooled mixed-phase clouds, the impacts of clouds on the radiation budget are very complex and poorly understood over the Arctic (Curry et al. 1996; Shupe and Intrieri 2004; Walsh et al. 2009).

Reanalysis datasets are convenient tools for studying Arctic cloud and radiation interactions, especially in data-sparse regions where in situ observations are difficult to obtain on account of the unique and extreme environments (Walsh et al. 2009). Specifically, a reanalysis combines an unchanging data assimilation scheme and model results with all available observations into a spatially complete gridded meteorological dataset, which provides a long-term representation of the state of the atmosphere (Dee et al. 2011). But the uncertainties of reanalyses should be quantified first in Arctic climate studies.

Several studies have evaluated the performance of reanalyses over the Arctic for different processes, such as upper-level winds (Bromwich and Wang 2005), tropospheric assessments (Bromwich et al. 2007), precipitation (Serreze and Hurst 2000), atmospheric moisture budgets (Bromwich et al. 2000, 2002), and overall assessments including surface temperature, radiative fluxes, wind speed, and precipitation (Lindsay et al. 2014). Other studies have focused on clouds and/or radiative fluxes. For example, Walsh et al. (2009) evaluated cloud and radiation properties in four reanalyses (NCEP-NCAR reanalysis, ERA-40, NARR, and JRA-25) using surface observations from the Atmospheric Radiation Measurement (ARM) Program Northern Slope of Alaska (NSA) site at Barrow, Alaska (BAR; now known as Utqiaġvik), from 1999 to 2006. The conclusion is that large seasonal cloud fraction (CF) biases have significant effects on the surface energy budget. Zib et al. (2012) conducted a study which evaluated reanalyzed cloud and radiation fields from five reanalyses (MERRA, CFSR, 20CR, ERA-Interim, and NCEP-DOE AMIP-II reanalysis) at BAR and Ny-Ålesund, Norway (NYA), using 15 years (1994–2008) of Baseline Surface Radiation Network (BSRN) observations. Their study suggests that radiative flux errors found in the reanalyses may not always be dependent on CF errors.

More recently, Liu and Key (2016) examined cloud cover anomalies in five reanalysis products. They concluded that all of reanalyses exhibit large

biases in winter and have better performance over land than over ocean. In this study, in addition to evaluating the reanalysis CF, we also conduct a thorough radiation evaluation as well as investigate how the cloud property biases contribute to radiation budget biases.

In this study, five contemporary global reanalyses are evaluated and intercompared: 1) the Japan Meteorological Agency (JMA)'s Japanese 55-Year Reanalysis (JRA-55); 2) the National Oceanic and Atmospheric Administration (NOAA)'s Twentieth Century Reanalysis, version 2c (20CRv2c); 3) the National Centers for Environment Prediction (NCEP)'s Climate Forecast System Reanalysis (CFSR); 4) the European Centre for Medium-Range Weather Forecasts (ECMWF) interim reanalysis (ERA-Interim); and 5) the National Aeronautics and Space Administration (NASA)'s Modern-Era Retrospective Analysis for Research and Applications, version 2 (MERRA-2). Compared to previous studies, NASA Clouds and the Earth's Radiant Energy System (CERES) satellite observations have been introduced in this study to evaluate the temporal variation and spatial distribution of these five selected reanalysis datasets over the Arctic. Note that the CERES satellite retrieval products used in this study are not assimilated by these five reanalyses. Cloud fraction, cloud water path (CWP), SW and LW radiation fluxes at the top of the atmosphere (TOA) and surface, as well as their cloud radiative effects (CREs), are examined in each reanalysis from March 2000 to February 2012 within the Arctic domain (70° – 90° N). To estimate the uncertainties of the CERES-Moderate Resolution Imaging Spectroradiometer (MODIS) (CM)-derived CFs and the five reanalyzed CFs over the Arctic, *CloudSat-Cloud-Aerosol Lidar and Infrared Pathfinder Satellite Observations* (CALIPSO) (CC) data are also used in this study.

2. Data and methodology

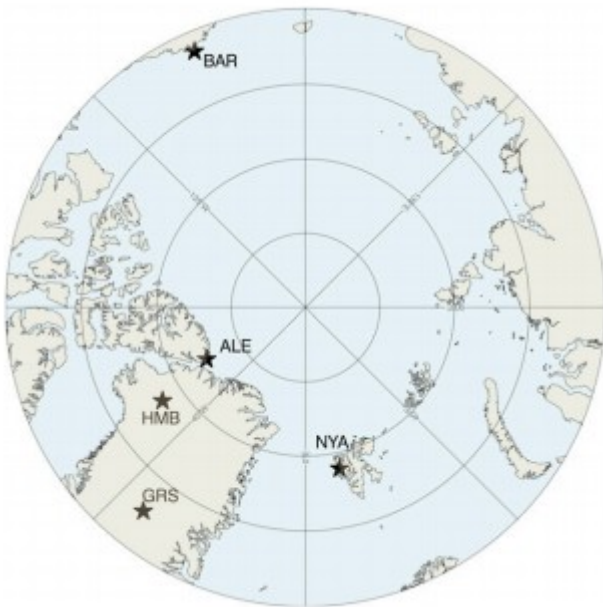
Twelve years of gridded monthly mean data from both CERES satellite products and reanalyses from March 2000 through February 2012 are bilinearly interpolated and regridded to the same spatial resolution ($2^{\circ} \times 2^{\circ}$) during the comparisons. Although CERES satellite products have a more complete temporal and spatial coverage, their uncertainties should first be estimated before using them as a reference to evaluate the reanalyzed results. Therefore, the CM-derived CFs (both temporal and spatial) are compared with the 4-yr CC observations, and CM-derived surface SW and LW fluxes are compared with the surface observations at five selected sites. These estimated uncertainties have been considered in reanalysis evaluation in section 3.

a. Surface observations

The five Arctic surface sites used for CERES validation are presented in Fig. 1. The CERES-derived Energy Balanced and Filled (EBAF) surface radiative fluxes are evaluated by the BSRN observations. BSRN was initiated to study the surface radiation budget and to provide a validation dataset for satellite radiometry and climate models (Ohmura et al. 1998). In this study, the

surface downward SW (SW_down) and downward LW (LW_down) radiative fluxes from three Arctic BSRN sites have been selected to evaluate the CERES EBAF. The three selected BSRN sites are Alert, Lincoln Sea, Canada (ALE; 82.49°N, 62.42°W); BAR (71.32°N, 156.61°W); and NYA (78.93°N, 11.93°E). Two non-BSRN sites, Humboldt Glacier, Greenland (HMB; 78.53°N, 56.83°W), and Greenland Summit, Greenland (GRS; 72.57°N, 38.48°W), are used for the validation as well. The five sites are scattered over the Arctic, providing a long-term dataset at a high temporal resolution (1 or 5 min) and a reasonable representation of Arctic land surface radiation. At the BAR site, the broadband SW_down (0.3–3 μm) and LW_down (4–50 μm) fluxes are measured by the Eppley Precision Spectral Pyranometer (PSP) and the Eppley Precision Infrared Pyrgeometer (PIR) with estimated uncertainties of 10 and 4 W m^{-2} , respectively (Dong et al. 2010). Kipp and Zonen pyranometers and Eppley PIRs are used for measuring SW_down and LW_down fluxes, respectively, at the ALE and NYA sites (Zib et al. 2012; Halliwell 2012).

Fig. 1. The Arctic domain (70°–90°N) considered in this study, and selected Arctic surface sites (black stars), including coordinates and available data time frame in parentheses: Barrow, Alaska (71.32°N, 156.61°W; SW and LW: March 2000–February 2015); Ny-Ålesund, Norway (78.93°N, 11.93°E; SW and LW: March 2000–March 2015); Alert, Lincoln Sea, Canada (82.49°N, 62.42°W; SW and LW: August 2004–March 2014); Humboldt Glacier, Greenland (78.53°N, 56.83°W; SW: March 2002–May 2013); and Greenland Summit, Greenland (72.57°N, 38.48°W; SW: March 2003–May 2013).



b. Satellite observations

1) CERES-MODIS SYN1deg edition 3A

This study uses 12 years of monthly mean CM 1° synoptic (SYN1deg) edition 3A gridded dataset (1° × 1°), which combines data from the *Aqua* and *Terra* satellites, for evaluating five reanalyzed CFs and CWPs. Details related to the

CM edition 2 retrieval methods for cloud properties can be found in Minnis et al. (2011a), and their uncertainties have been quantified using ARM ground-based observations and/or satellite retrievals (Dong et al. 2008, 2016; Xi et al. 2010, 2014; Minnis et al. 1999, 2002, 2011b).

According to Minnis et al. (2008), the CM *Aqua* and *Terra* CF retrievals have been extensively compared with other observations and they found a 7% uncertainty in CM global CF retrievals. The global mean total CF from CM edition 2 is the lowest among 12 different satellite retrievals (Stubenrauch et al. 2013), whereas its low- and high-level CFs are close to the averages of the 12 datasets. Thus, other than having lower midlevel CFs than all other retrievals except for *CALIPSO*, the CM-derived CFs are representative of passive satellite cloud amounts globally. For single-layer cirrus clouds, Mace et al. (2005) found that the CM-derived ice water paths (IWPs) were $3.3 \pm 16.2 \text{ g m}^{-2}$ less than the IWPs derived from ground-based radar. Roughly, the mean CM IWP for all ice clouds is similar to the mean IWP from *CloudSat* in both magnitude and distribution (Waliser et al. 2009; Stanfield et al. 2014). Over the Arctic, the CM-derived IWPs are compared with the *CloudSat* and *CALIPSO* level-2C ice cloud property product (2C-ICE; Deng et al. 2015); their summer (JJA) mean values over the Arctic from 2006 to 2010 are 74.2 and 78.6 g m^{-2} (not shown), respectively.

Minnis et al. (2011b) found that the CM-derived global mean liquid water path (LWP) over the ocean has a mean bias of -0.2 g m^{-2} and a standard deviation of 53.6 g m^{-2} ($R^2 = 0.59$) compared to matched overcast *Aqua* Advanced Microwave Scanning Radiometer for Earth Observing System (AMSR-E) footprints. Over the Arctic, Dong et al. (2016) compared the CM-retrieved LWPs over snow-free and snow conditions with ARM NSA ground-based retrievals over the period of March 2000–December 2006. Mean differences and correlation coefficients R of the CM-retrieved LWPs relative to ARM-retrieved LWPs are -0.6 g m^{-2} and 0.73 under snow-free conditions (surface albedo $R_{\text{sfc}} \leq 0.3$) and 5.6 g m^{-2} and 0.59 for snow cases ($R_{\text{sfc}} > 0.3$).

2) CERES EBAF-TOA and EBAF-surface edition 2.8

The CERES EBAF-TOA and EBAF-surface radiative fluxes, which are also monthly mean gridded ($1^\circ \times 1^\circ$) datasets, are both used in this study to evaluate reanalyzed radiative fluxes. In the EBAF product, the CERES SW and LW fluxes are adjusted within their measurement uncertainties such that the CERES long-term global annual mean net flux is consistent with the long-term annual mean ocean heat storage data (Loeb et al. 2009). EBAF-surface fluxes are calculated using the NASA Langley modified Fu-Liou radiative transfer model with inputs from CM-retrieved cloud properties, meteorological data from a reanalysis system, and aerosol data from an aerosol assimilation system. CERES-observed TOA irradiances are used to constrain surface irradiance computations such that the computed TOA irradiances are consistent with CERES TOA observations.

The regional uncertainties of CERES EBAF-TOA SW and LW fluxes are summarized by the CERES science team as follows: clear-sky LW_{up} flux (3.6 W m⁻²), clear-sky SW_{up} flux (2.6 W m⁻²), all-sky LW_{up} flux (2 W m⁻²), and all-sky SW_{up} flux (~5 W m⁻² for March 2000–June 2002 and ~4 W m⁻² for July 2002–December 2010) (CERES 2014). Kato et al. (2013) compared the calculated EBAF-surface radiative fluxes with the surface observations at 24 surface sites and made the following conclusions: the biases [root-mean-square differences (RMSDs)] for SW_{down} flux are –1.7 (7.8) W m⁻² over land and 4.7 (13.3) W m⁻² over ocean, while for LW_{down} flux they are –1.0 (7.6) W m⁻² over land and –2.5 (13.3) W m⁻² over ocean (CERES 2015). However, these estimations mainly focused on the tropical and midlatitude sites. Therefore, it is necessary to estimate the uncertainties of CERES EBAF-surface radiative fluxes over the Arctic.

The seasonal and annual mean biases of surface SW_{down} and LW_{down} fluxes from CERES EBAF-surface against the Arctic surface observations are summarized in Table 1. The monthly mean radiative fluxes at each site were obtained from the CERES EBAF validation web page (<http://www-cave.larc.nasa.gov/pages/sfcobs.html>), where the temporal averaging methodology can be found in Rutan et al. (2001). Compared to the surface SW_{down} flux measurements at five selected sites, the CERES-derived SW_{down} flux has positive biases (RMSDs) of +8.86 (9.06) W m⁻², +0.12 (1.58) W m⁻², and +2.27 (4.91) W m⁻² for summer, winter, and annual mean, respectively. As for the surface LW_{down} flux, its biases (RMSDs) are +0.88 (2.05) W m⁻², +6.46 (6.47) W m⁻², and +4.41 (6.17) W m⁻² for summer, winter, and annual mean, respectively. Although the biases are relatively large for specific season(s), the average monthly mean differences are lower than the estimated uncertainties of monthly gridded irradiances as presented in Kato et al. (2013). Christensen et al. (2016) concluded that CERES EBAF-surface should be considered as a key benchmark for evaluating the Arctic surface radiation budget, as they found smaller RMSDs than the expected uncertainties by Kato et al. (2013) (Boeke and Taylor 2016). However, the uncertainties of CERES EBAF-surface could be higher over the ocean or other surface types lacking surface validation.

TABLE 1. Seasonal and annual biases and RMSDs (in parentheses) of CM-derived surface radiative fluxes against the surface observations (averages from BAR, NYA, ALE, GRS, and HMB) within the Arctic (70°–90°N).

	Surface SW _{down} flux (W m ⁻²)	Surface LW _{down} flux (W m ⁻²)
DJF	+0.12 (1.58)	+6.46 (6.47)
MAM	–1.34 (2.35)	+8.94 (9.76)
JJA	+8.86 (9.06)	+0.88 (2.05)
SON	+1.42 (2.94)	+1.35 (3.33)
Annual	+2.27 (4.91)	+4.41 (6.17)

3) Combined *CloudSat-CALIPSO-CERES-MODIS* data product

Because of the large uncertainty of derived cloud properties from passive remote sensors over the Arctic, we consider active remote sensor CC-derived CFs as a ground truth to validate the CFs derived from CM and five reanalyses in this study. The CALIOP and cloud parameter retrievals from July 2006 to June 2010 obtained from the combined *CloudSat-CALIPSO-CERES-MODIS* (CCCM; Kato et al. 2010) release 1B (Rel1B) data product are used for total column CF comparisons (see Figs. 2 and 6).

c. Global reanalyses

Table 2 provides a general overview of the most recent versions of the global reanalyses explored in this study.

TABLE 2. Basic characteristics of the five selected reanalyses. (For model resolution, Txxx denotes spectral horizontal resolution with triangular truncation at wavenumber xxx, and Lxx denotes xx vertical levels/layers.)

	JRA-55	20CRv2c	CFSR	ERA-Interim	MERRA-2
Model resolution	T319 L60	T62 L28	T382 L64	T255 L60 and N128 reduced Gaussian grid	72 sigma levels
Grid spacing (lon × lat)	1.25° × 1.25°	2° × 2°	0.31° × 0.31°	0.75° × 0.75°	0.625° × 0.5°
Assimilation method	4D-Var	Ensemble Kalman filter	3D-Var	4D-Var	3D-Var
Temporal range	Jan 1958–present	Jan 1851–Dec 2014	Jan 1979–present	Jan 1979–present	Jan 1980–present
Sea ice and SST	COBE-SST	COBE-SST2	Reynolds SST (after October 1981); various interactive	NCEP and Operational Sea Surface Temperature and Sea Ice Analysis (OSTIA) (Feb 2009–present)	CMIP (Jan 1980–Dec 1981), Reynolds SST (Jan 1982–Mar 2006), and OSTIA (Apr 2006–present)
Solar constant (W m ⁻²)	1365	Annually varied from 1366 W m ⁻² (Van den Dool 2011)	Annually varied from 1366 W m ⁻² (Van den Dool 2011)	1370	1365
Cloud property parameterizations	Sommeria and Deardorff (1977)	Xu and Randall (1996)	Xu and Randall (1996)	Tiedtke (1993)	Bacmeister et al. (2006)
Radiative properties parameterizations	LW (Chou et al. 2001) SW (JMA 2013)	LW (Mlawer et al. 1997) SW (Hou et al. 2002)	LW (Fels and Schwarzkopf 1975; Schwarzkopf and Fels 1991) SW (Chou et al. 1998; Hou et al. 1996, 2002)	LW and SW (Mlawer et al. 1997)	LW (Chou et al. 2001) SW (Chou and Suarez 1999)
References	Kobayashi et al. (2015)	Compo et al. (2011)	Saha et al. (2010)	Dee et al. (2011)	Rienecker et al. (2011) and Bosilovich et al. (2015)

1) JMA JRA-55

JMA conducted the second Japanese global atmospheric reanalysis, called JRA-55, based on the TL319 spectral resolution version of the JMA global spectral model (GSM). It provides information back to 1958, when regular

radiosonde observations started becoming available globally. The sea ice albedo is a function of solar zenith angle and skin temperature in the model used in the JRA-55 (Kobayashi et al. 2015).

2) NOAA-CIRES 20CRv2c

20CR was generated by assimilating surface pressure, sea surface temperatures, and sea ice distributions as boundary conditions using the ensemble Kalman filter method (Whitaker and Hamill 2002). 20CRv2c used the same model as the NCEP Global Forecast System (GFS) 2008 experimental (2008ex) (Compo et al. 2011), version 2, but involved new sea ice boundary conditions from the Centennial in situ Observation-Based Estimates with updated SST (COBE-SST2; Hirahara et al. 2014), new pentad Simple Ocean Data Assimilation with the input of sea surface temperature fields (SODAsi.2), and additional observations from International Surface Pressure Databank (ISPD), version 3.2.9 (NCAR 2015). Recent updates to the GFS can be found in Moorthi et al. (2001).

3) NCEP CFSR

The CFSR, undertaken by the NCEP, covers the modern satellite era from 1979 to the present based on a fully coupled atmosphere-ocean-land model and the three-dimensional variational data assimilation (3D-Var) technique (Saha et al. 2006, 2014). Comparing with previous reanalysis in NCEP, a sea ice merging scheme is used in the CFSR to add sea ice concentration into the system, which generates more realistic interactions between sea ice and the atmosphere in the polar regions (Wu and Grumbine 2013).

4) ERA-Interim

ERA-Interim is produced with the ECMWF Integrated Forecast System (IFS), a forecast model with three fully coupled components for the atmosphere, land surface, and ocean waves. In addition, the 12-hourly four-dimensional variational data assimilation (4D-Var) of the upper-air atmospheric state is the key component of its data assimilation system (Dee et al. 2011). For sea ice, monthly mean albedos based on Ebert and Curry (1993) are used for the Arctic Ocean. A bare sea ice albedo value is applied for summer, while a dry snow albedo is applied during winter. In addition, the different albedo values at visible and near-infrared spectral bands are also considered (ECMWF 2014).

5) NASA MERRA-2

MERRA-2 is a reanalysis using a recent version of the Goddard Earth Observing System Model, version 5 (GEOS-5), Data Assimilation System covering the modern satellite era. The MERRA-2 reanalysis includes updates to dynamics, physics, and aerosol assimilation and incorporates more satellite observations than the MERRA reanalysis. In MERRA-2, the sea ice albedo is now seasonally prescribed whereas this value was fixed as a

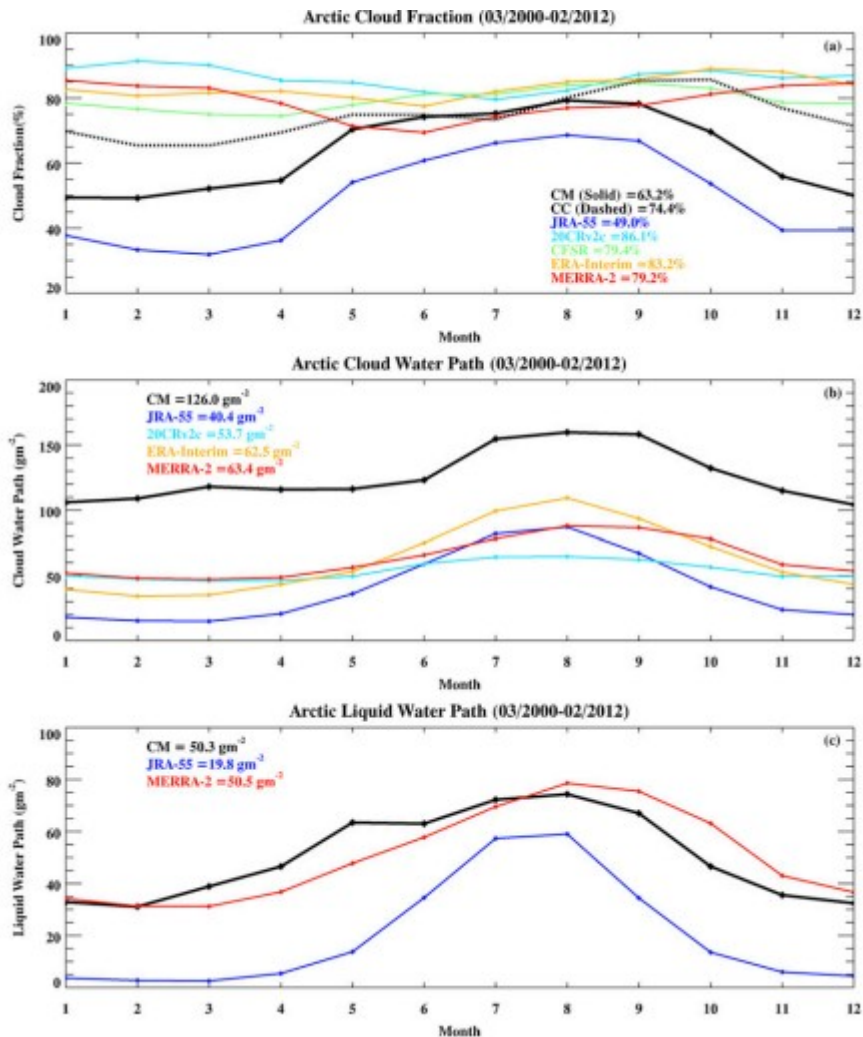
constant of 0.6 in the MERRA reanalysis (Rienecker et al. 2011; Bosilovich et al. 2015).

3. Results and discussion

a. Monthly mean comparison

As mentioned before, the five selected reanalyses use different parameterizations to generate cloud properties in their models, which creates large discrepancies in the seasonal cycle as illustrated in Fig. 2a. The active satellite product CC-derived CFs range from 65.4% in February to 85.7% in October with an annual mean of 74.4% over the period of 2006–10. The seasonal variations of CFs in MERRA-2, CFSR, ERA-Interim, and 20CRv2c resemble that of CC. In terms of monthly means, all reanalyses except for JRA-55 agree well with CC from May to September, but overestimate CF from October to April, resulting in positive biases ranging from +4.8% (MERRA-2) to +11.7% (20CRv2c). JRA-55 CFs have a relatively large negative bias (−25.4%) compared to the annual mean (74.4%) from CC-derived CFs. Recently, Liu and Key (2016) performed an Arctic cloud amount assessment on five reanalysis products using MODIS and *CALIPSO* observations, and also concluded that reanalysis products exhibit a large bias in cloud amount in the winter. However, English et al. (2014) discussed that Arctic clouds during the wintertime are near the surface and/or too optically thin to be observed by *CALIPSO*, which may lead to an unfair comparison between native model output and observations. Using Cloud Feedback Model Intercomparison Project (CFMIP) Observation Simulator Package (COSP) could be a potential way to make this comparison in a more consistent way. Using the *CALIPSO* instrument simulator, the Arctic winter clouds in the Community Atmosphere Model, version 5 (CAM5), can be reduced by 20%–30% from native model output, as mentioned in English et al. (2014), which may explain large positive biases of winter clouds in these global reanalyses. Therefore, Arctic wintertime cloud amount cannot be confidently evaluated until instrument simulators are implemented in reanalysis products (Bodas-Salcedo et al. 2011).

FIG. 2. Monthly means of (a) CF, (b) CWP, and (c) LWP from CM SYN1deg and available reanalyses during the period of March 2000–February 2012. CC data is included in (a) during the period 2006–10. Annual means are provided for each dataset and variable.



Compared to CC, the CM-derived CFs over the period of 2000–12 have a negative bias of -11.2% for annual mean, with almost identical values in summer (within $\pm 2\%$), but a large negative bias ($\sim -20\%$) from October to April, indicating that the CM-derived CFs are reliable in summer but not in winter. Note that the terms summer and winter used in this study represent June, July, and August (JJA) and December, January, and February (DJF), respectively. This is consistent with the conclusion in Kay and L'Ecuyer (2013) that MODIS underestimates Arctic cloud amounts, especially in winter. It is well known that passive remote sensors have difficulties with distinguishing clouds from the highly reflective snow/ice surfaces underneath without solar radiation during the winter. Liu and Key (2016) found that CALIPSO-derived CFs from 2006 to 2014 are consistently higher than those derived from Terra MODIS by 7.7%, which is slightly different from our conclusion. The difference is mainly attributed to different Arctic domains (60°N northward vs 70°N northward) and different MODIS products (Terra MODIS results by the MODIS team versus Terra/Aqua MODIS results by the CERES team) used in these two studies. Our analysis indicates that CM

winter CFs are lower than *Terra* MODIS, and both CC and CM CFs are lower for 70°N northward domain compared to the larger Arctic domain (60°N northward).

The monthly mean CWP (LWP + IWP) values derived from CM range from 107 to 160 g m⁻² with an annual mean of 126 g m⁻² as shown in Fig. 2b. Compared to CM-derived CWPs (126 g m⁻²), the MERRA-2 and ERA-Interim reanalyzed CWPs are about half (62.5 and 63.4 g m⁻², respectively) of the observed, whereas 20CRv2c and JRA-55 reanalyzed CWPs are even lower (53.7 and 40.4 g m⁻², respectively). Figure 2c shows that the monthly mean LWP in MERRA-2 is nearly identical to that of CM. Therefore, we can conclude that the CWP bias in MERRA-2 is primarily due to the underestimation in IWP over the Arctic, while the CWP bias in JRA-55 is caused by the wrong representation of both IWP and LWP. English et al. (2015) found that insufficient liquid water is the one of main reasons for LW biases in models from phase 5 of the Coupled Model Intercomparison Project (CMIP5), especially at mixed-phase cloud temperatures (Komurcu et al. 2014).

Figure 3 illustrates the monthly mean TOA reflected shortwave (SW_{up}) and outgoing longwave (LW_{up}) fluxes under all-sky and clear-sky conditions. The biases and RMSDs of the seasonal and annual means in the TOA radiative fluxes and CREs are also given in Table 3. Note that the solar constants in five reanalyses are a few watts per meter squared higher than the CERES EBAF counterpart (1361 W m⁻²) as shown in Table 2. The seasonal variations of all-sky TOA SW_{up} fluxes (SW_{all}^{\uparrow}) are primarily determined by the seasonal changes in the intensity and duration of insolation, and partially determined by CF, cloud optical properties and surface albedo. The annual mean differences range from -6.5 W m⁻² in JRA-55 to +3.9 W m⁻² in MERRA-2 compared with CERES EBAF (99.6 W m⁻²). However, their monthly mean differences vary significantly from a few watts per meter squared (September–April) to approximately 30 W m⁻² (May–July). The relatively large negative bias in JRA-55 is likely due to the underestimation of both CF and LWP, while the relatively smaller biases in the other four reanalyses are due to the compensating effects of overestimated CF and underestimated CWP in summer. The seasonal variations in the observed clear-sky TOA SW_{up} flux are similar to its all-sky counterpart, but the annual mean (80.1 W m⁻²) is approximately 20 W m⁻² lower than the all-sky condition and peaks in May because of the high solar radiation and large snow and/or ice coverage. The reanalyzed monthly means of clear-sky SW_{up} fluxes (SW_{clr}^{\uparrow}) agree with CERES EBAF results within 10 W m⁻² except for JRA-55 from May to June. Under clear-sky conditions, the sea ice albedo could be a potential problem for reanalyses because it is typically prescribed in the model. The sea ice albedo is roughly 0.7 from March to May and can be as low as 0.2–0.3 in August and September according to CM retrievals. However, all reanalyses tend to underestimate sea ice albedo from March to July, and overestimate it after August (not shown). Therefore, the underestimation of the clear-sky

SW_{up} flux in JRA-55 is presumably caused by its low surface albedo throughout the year. Note that the TOA clear-sky SW_{up} and LW_{up} fluxes are not available for the 20CRv2c.

FIG. 3. Monthly means of TOA fluxes for (a) all-sky SW_{up}, (b) clear-sky SW_{up}, (c) all-sky LW_{up}, and (d) clear-sky LW_{up} from CERES EBAF and five selected reanalyses during the period of March 2000–February 2012. Annual means are provided for each dataset and variable.

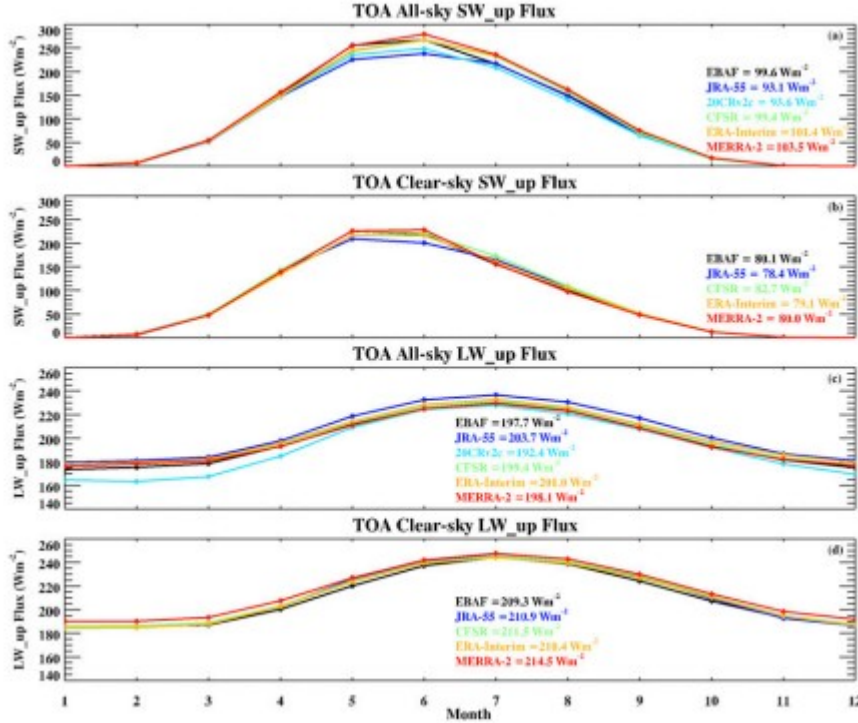


TABLE 3. The biases and RMSDs (in parentheses) of seasonal and annual means of TOA radiation fluxes and CREs from five selected reanalyses compared with CERES EBAF results.

Variables		CERES EBAF	JRA-55	20CRv2c	CFSR	ERA-Interim	MERRA-2
LW _{all} ⁱ (W m^{-2})	DJF	174.67	+5.80 (6.60)	-8.90 (9.95)	+2.60 (3.62)	+4.40 (5.31)	+2.46 (3.52)
	JJA	226.70	+6.50 (6.74)	-2.40 (2.87)	+1.00 (2.33)	+2.50 (2.76)	-1.00 (1.98)
	Annual	197.68	+6.07 (6.52)	-5.24 (7.17)	+1.76 (2.92)	+3.33 (4.10)	+0.37 (2.53)
SW _{all} ⁱ (W m^{-2})	DJF	2.70	-0.53 (0.80)	-0.47 (0.62)	-0.53 (0.76)	-0.10 (0.29)	-0.50 (0.68)
	JJA	211.40	-9.87 (23.40)	-12.40 (24.67)	+7.57 (19.67)	+10.40 (21.24)	+14.40 (20.44)
	Annual	99.58	-6.50 (14.88)	-5.97 (14.34)	-0.18 (11.40)	+1.77 (12.01)	+3.92 (11.46)
LW _{clr} ⁱ (W m^{-2})	DJF	186.07	-0.63 (2.47)	—	+0.67 (3.32)	-0.67 (4.54)	+4.63 (7.66)
	JJA	240.20	+2.37 (5.03)	—	+2.10 (4.71)	+0.87 (4.58)	+4.00 (6.36)
	Annual	209.27	+1.62 (4.08)	—	+2.27 (4.26)	+1.14 (4.74)	+5.28 (7.60)
SW _{clr} ⁱ (W m^{-2})	DJF	2.37	-0.30 (0.61)	—	-0.27 (0.60)	-0.17 (0.47)	-0.47 (0.82)
	JJA	157.77	-0.50 (26.07)	—	+9.90 (27.58)	+2.87 (19.60)	+2.73 (23.22)
	Annual	80.09	-1.69 (14.65)	—	+2.59 (15.97)	-0.96 (11.87)	-0.13 (14.71)
CRE _{LW} (W m^{-2})	DJF	11.40	-6.40 (7.18)	—	-1.93 (3.20)	-5.03 (5.92)	+2.17 (5.29)
	JJA	13.50	-4.13 (5.13)	—	+1.10 (4.23)	-1.63 (4.13)	+5.00 (6.94)
	Annual	11.58	-4.44 (5.46)	—	+0.52 (3.49)	-2.19 (4.38)	+4.92 (7.14)
CRE _{SW} (W m^{-2})	DJF	-0.33	+0.23 (0.48)	—	+0.27 (0.50)	-0.07 (0.37)	+0.03 (0.35)
	JJA	-53.63	+9.37 (17.20)	—	+2.33 (16.00)	-7.53 (18.29)	-11.67 (18.90)
	Annual	-19.48	+4.81 (10.77)	—	+2.76 (10.67)	-2.75 (10.02)	-4.06 (10.84)
CRE _{NET} (W m^{-2})	DJF	11.07	-6.17 (7.06)	—	-1.67 (3.16)	-5.10 (5.99)	+2.20 (5.33)
	JJA	-40.13	+5.23 (15.47)	—	+3.43 (16.67)	-9.17 (18.21)	-6.67 (17.55)
	Annual	-7.90	+0.37 (10.80)	—	+3.28 (11.74)	-4.93 (10.73)	+0.86 (11.91)

The monthly means of all-sky TOA LW_{up} fluxes from CERES observations and reanalyses monotonically increase from about 175 W m⁻² in January to about 232 W m⁻² in July and then decrease into the following winter. The all-sky LW_{up} fluxes (LW_{all}^{\uparrow}) are strongly influenced by variations in CF, CWP, cloud-top temperature, emissivity, and surface temperature (Dong et al. 2006, 2010). The monthly means of all-sky LW_{up} fluxes in CFSR, ERA-Interim, and MERRA-2 agree well with the CERES EBAF results (197.7 W m⁻²) with annual mean differences of 1.8, 3.3, and 0.4 W m⁻², respectively. The JRA-55 has a positive bias of 6 W m⁻² in the annual mean, which is consistent with its lower CF and CWP; the surface will contribute more to the TOA LW_{up} flux. The annual mean clear-sky TOA LW_{up} flux from CERES EBAF is 209.3 W m⁻², which is 12 W m⁻² greater than its all-sky counterpart. The clear-sky LW_{up} flux (LW_{clr}^{\uparrow}) differences between reanalyses and CERES EBAF are within 5 W m⁻² through the year. In general, all reanalyses capture the seasonal variations of CERES EBAF derived TOA LW_{up} fluxes under both all-sky and clear-sky conditions.

The CREs are introduced to quantify the overall effect of clouds on the radiation budget, which can be calculated by the following equations. The net CRE is the sum of the SW and LW CREs:

$$\begin{aligned} CRE_{SW}(TOA) &= (SW^{\downarrow} - SW_{all}^{\uparrow}) - (SW^{\downarrow} - SW_{clr}^{\uparrow}) \\ &= SW_{clr}^{\uparrow} - SW_{all}^{\uparrow}, \\ CRE_{LW}(TOA) &= (LW_{all}^{\downarrow} - LW_{all}^{\uparrow}) - (LW_{clr}^{\downarrow} - LW_{clr}^{\uparrow}) \\ &= LW_{clr}^{\uparrow} - LW_{all}^{\uparrow}, \quad \text{and} \\ CRE_{NET}(TOA) &= CRE_{SW} + CRE_{LW}. \end{aligned}$$

The LW, SW, and net CRE monthly means are presented in Fig. 4. The monthly mean SW CREs (Fig. 4a) in CERES EBAF are negative throughout the year with a peak in July, indicating a radiative energy loss (cooling effect). Compared to the observed annual mean SW CRE (−19.5 W m⁻²), reanalyzed SW CREs essentially follow the observed seasonal variation with annual biases ranging from +4.8 W m⁻² in JRA-55 to −4.1 W m⁻² in MERRA-2. In contrast to the SW radiative cooling effect, the observed LW CREs (Fig. 4b) are positive throughout the year and increase from 6.8 W m⁻² in April to 15.4 W m⁻² in August, indicating a warming effect (energy gain). The seasonal variations in the reanalyzed LW CREs mimic the CERES EBAF variation, and their annual and monthly means agree with the CERES EBAF observations within ±5 W m⁻², peaking in September. Compared to the SW CRE, the magnitudes of the LW CRE are much smaller in the summer. Similar results were found in CMIP5 when compared with CERES EBAF (English et al. 2015). The Arctic net CRE (Fig. 4c) is dominated by the LW warming effect during the winter and by the SW cooling effect during the summer. The annual mean net CRE from CERES EBAF is −7.9 W m⁻², while the reanalyses range from −4.6 W m⁻² in CFSR to −12.8 W m⁻² in ERA-Interim, indicating that

clouds have a net cooling effect on the TOA radiation budget over the Arctic. There is a better agreement between the reanalyses and observations in the net CRE, which is due to a compensating effect when combining LW and SW CREs.

FIG. 4. Monthly means of TOA (a) SW, (b) LW, and (c) net CREs from CERES EBAF and four available reanalyses during the period of March 2000–February 2012. Annual means are provided for each dataset and variable.

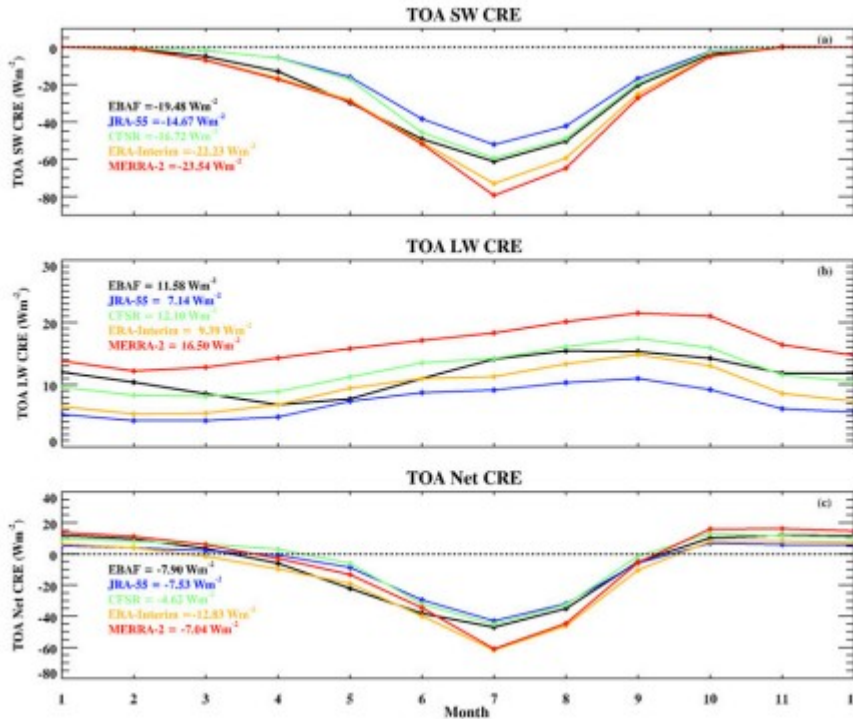


Figure 5 shows the monthly means of all-sky radiative fluxes at the surface from CERES EBAF and the five selected reanalyses. The annual means of SW_down and SW_up fluxes from CERES EBAF-surface are 95.9 and 53.9 W m⁻², respectively, with SW_down flux peaking in June whereas the maximum SW_up flux is in May due to the relatively high surface albedo from large snow and/or ice coverage (Dong et al. 2010; Wang and Key 2005). As presented in Fig. 5a and listed in Table 4, the CFRS and ERA-Interim reanalyzed SW_down fluxes have negative biases of -11.9 and -24.1 W m⁻² in summer, presumably because the positive CF biases have more weight than the negative CWP biases. However, the large negative bias in MERRA-2 (-23.7 W m⁻²) is not consistent with its negative biases of both CWP and CF during summertime. Note that SW_down flux from CERES EBAF is approximately 8.9 W m⁻² higher than the land surface observations during the summer as shown in Table 1. Thus, the negative biases from these three reanalyses could be much lower than those shown in Fig. 5 after considering the bias in CERES EBAF-surface SW fluxes.

FIG. 5. Monthly means of (a) SW_down, (b) SW_up, (c) LW_down, and (d) LW_up fluxes at the surface from CERES EBAF-surface and five selected reanalyses during the period of March 2000–February 2012. Annual means are provided for each dataset and variable.

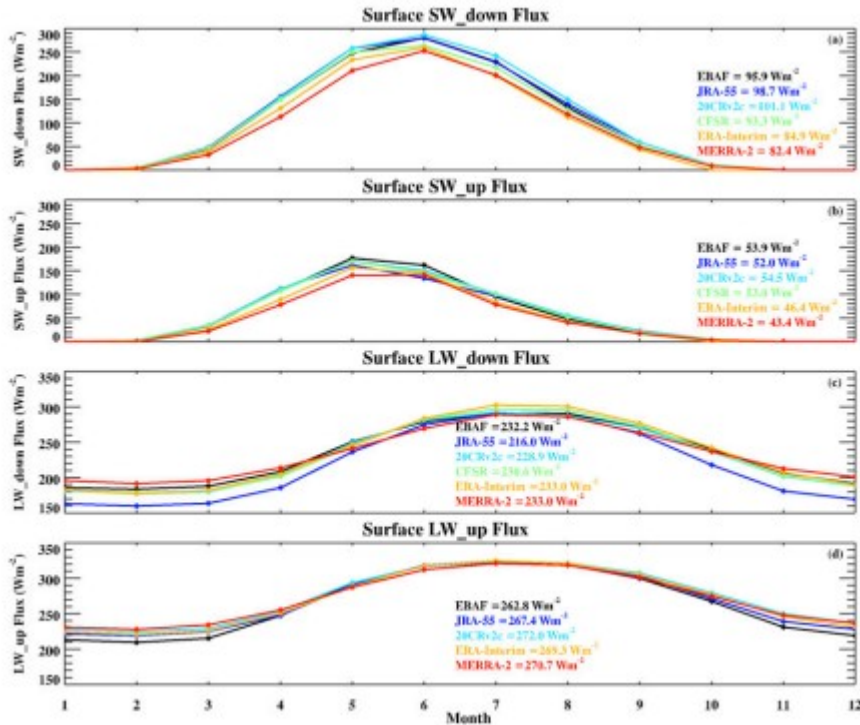


TABLE 4. As in Table 3, but for the surface radiative fluxes.

Variables		CERES EBAF	JRA-55	20CRv2c	CFSR	ERA-Interim	MERRA-2
LW_{all}^{\uparrow} ($W m^{-2}$)	DJF	213.67	+9.23 (11.45)	+16.07 (19.51)	—	+11.70 (16.33)	+18.10 (22.94)
	JJA	319.47	+1.90 (5.61)	+1.07 (7.26)	—	+1.57 (6.13)	-2.30 (6.40)
	Annual	262.84	+4.58 (8.67)	+9.19 (14.98)	—	+6.49 (12.88)	+7.84 (16.28)
LW_{dir}^{\uparrow} ($W m^{-2}$)	DJF	187.13	-23.03 (25.66)	-4.80 (8.63)	-3.73 (9.39)	-3.80 (10.56)	+8.90 (14.87)
	JJA	286.93	-2.37 (6.51)	+0.03 (9.20)	+4.97 (10.19)	+8.67 (16.68)	-5.56 (9.22)
	Annual	232.23	-16.22 (20.80)	-3.29 (9.20)	-1.64 (10.22)	+0.76 (12.83)	+0.81 (12.18)
SW_{all}^{\uparrow} ($W m^{-2}$)	DJF	0.87	+0.23 (0.55)	+0.27 (0.71)	+0.20 (0.56)	-0.87 (0.36)	-0.87 (0.00)
	JJA	101.13	-6.33 (27.49)	+1.13 (22.84)	-2.13 (24.34)	-11.13 (32.98)	-14.63 (25.06)
	Annual	53.87	-1.88 (15.51)	+0.66 (12.52)	-0.88 (14.52)	-7.46 (19.80)	-10.52 (20.31)
SW_{dir}^{\uparrow} ($W m^{-2}$)	DJF	1.57	+0.07 (0.55)	+0.07 (0.56)	0.0 (0.43)	-1.57 (0.42)	-0.47 (0.87)
	JJA	214.53	+1.17 (18.99)	+11.73 (22.93)	-11.83 (24.12)	-24.13 (45.58)	-23.67 (35.41)
	Annual	95.9	+2.8 (12.02)	+5.2 (13.60)	-2.6 (13.33)	-11.0 (25.72)	-13.5 (25.61)
LW_{dir}^{\downarrow} ($W m^{-2}$)	DJF	156.33	-6.30 (7.72)	—	-2.23 (4.63)	—	-9.10 (9.74)
	JJA	242.73	-1.60 (5.20)	—	-2.30 (5.86)	—	-5.06 (6.78)
	Annual	192.72	-3.92 (6.78)	—	-1.78 (5.27)	—	-7.26 (8.66)
SW_{dir}^{\downarrow} ($W m^{-2}$)	DJF	2.53	-0.77 (1.38)	—	-0.70 (1.30)	—	-0.83 (1.43)
	JJA	295.77	+0.77 (13.50)	—	+6.10 (11.13)	—	+2.23 (14.55)
	Annual	127.93	-1.59 (8.82)	—	+1.03 (6.65)	—	-2.39 (12.11)

As for the surface SW_up flux, the annual mean from CERES EBAF-surface is $53.9 W m^{-2}$ with a peak in May; the JRA-55, 20CRv2c, and CFSR annual means agree with CERES within $2 W m^{-2}$, while MERRA-2 and ERA-Interim have negative biases of -10.4 and $-7.5 W m^{-2}$, respectively. Reanalysis surface LW_up fluxes agree very well with their CERES EBAF-surface counterpart from April to October, but are consistently higher from

November to March. The LW_{down} fluxes from CERES monotonically increase from winter to July–August with an annual mean of 232.2 W m^{-2} . The annual means of LW_{down} fluxes from all reanalyses agree with CERES within $\pm 4 \text{ W m}^{-2}$, except for JRA-55, which has a negative bias of -16.2 W m^{-2} . In general, reanalyses generate too little LW_{down} flux during the winter compared to the summer, especially for JRA-55, which has a negative bias of -23.0 W m^{-2} in winter. This is consistent with the conclusions in Boeke and Taylor (2016) and Karlsson and Svensson (2011), where they indicated that this problem may be attributed to the cold Arctic atmosphere, low emissivity, or cloud errors in models. Generally, the negative bias in LW_{down} flux and the positive bias in SW_{down} from JRA-55 are consistent with its negative biases in CF and CWP.

b. Spatial distribution during summer (JJA)

As shown in Fig. 2a, the monthly means of CFs derived from CM are in good agreement with CC in the summer. To further demonstrate the spatial distributions of CF from these two datasets, we show summertime (JJA) means and differences over the Arctic from 2006 to 2010 in Fig. 6. The maximum CFs ($>90\%$) occurred in both datasets over the Atlantic side of the Arctic Ocean, as North Atlantic cyclones frequently track and advect warm/moist air to this region. In contrast, the CFs over Greenland and Ellesmere Island are minimal ($<60\%$) because these regions are dominated by a more stable boundary layer and anticyclonic weather systems (Serreze et al. 1998). However, CM tends to overestimate CF over the ocean by 6%–10% and underestimate CF over the land, especially over Greenland by about -10% . Considering the more complete spatial coverage and longer temporal record (2000–12) of the CM dataset, we will mainly focus on its cloud and radiation properties, as well as their interactions during the summertime in the following sections, during which the satellite retrievals are considered more reliable. The CF spatial differences between CM and CC will be considered when we use CM-derived CFs to evaluate reanalysis.

FIG. 6. Spatial distributions of the monthly mean CF during the summer (JJA) from (a) CM SYN1deg and (b) CC and (c) the bias of CM during the period of 2006–10, given as CM minus CC. The summer mean value is averaged from 70° to 82°N for each dataset.

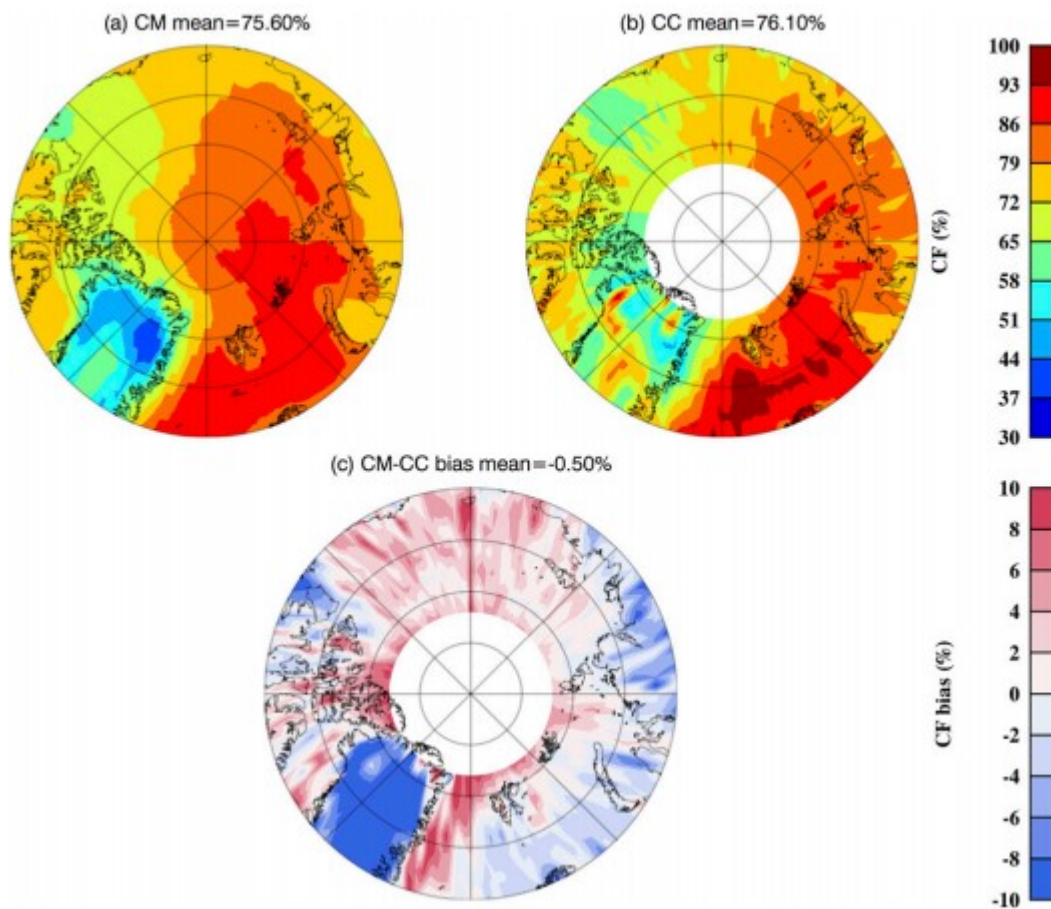


Figure 7 shows the average CF distribution over the Arctic with a mean value of 76.3% from CM and corresponding biases from the five reanalyses during the summertime from 2000 to 2012. The CF differences between reanalyses and CM shows that 20CRv2c, CFSR, and ERA-Interim have relatively large positive biases over the Arctic Ocean. However, the magnitudes of positive biases might be even larger if we recall the 6%–10% bias over the Ocean in CM. On the other hand, CFSR and MERRA-2, and especially JRA-55, may underestimate CF over the Greenland considering the –10% bias in CM, while 20CRv2c may not significantly overestimate CF over this region. The RMSDs of summer CFs in five reanalyses are 12.40%, 10.06%, 11.36%, 11.56%, and 7.05% for JRA-55, 20CRv2c, CFSR, ERA-Interim, and MERRA-2, respectively (not shown). The RMSD in JRA-55 is relatively close to its bias, indicating that there is a negative offset across most of the Arctic.

FIG. 7. Spatial distributions of (a) monthly mean CF during the summer (JJA) from CM SYN1deg and (b)–(f) the associated biases from five selected reanalyses, given as the reanalysis minus CM SYN1deg.

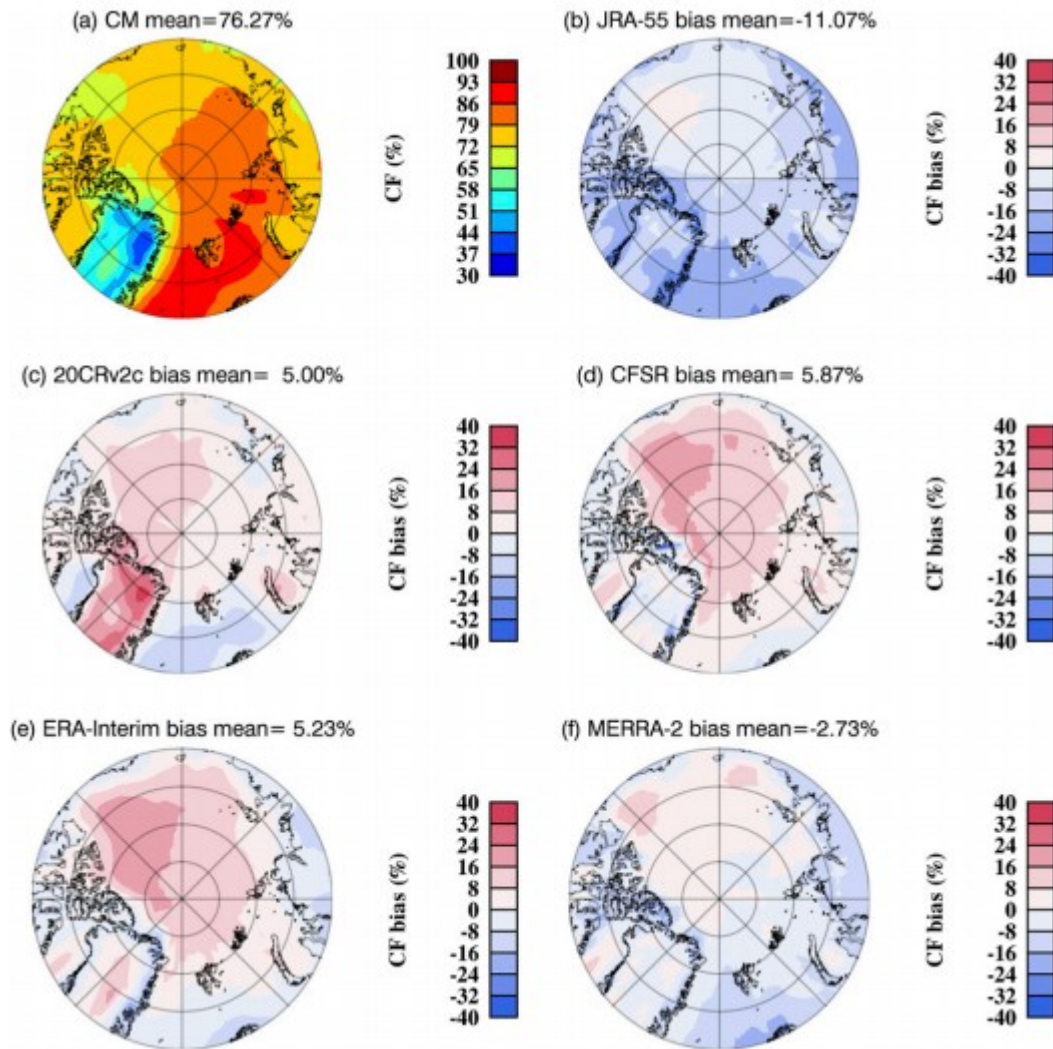
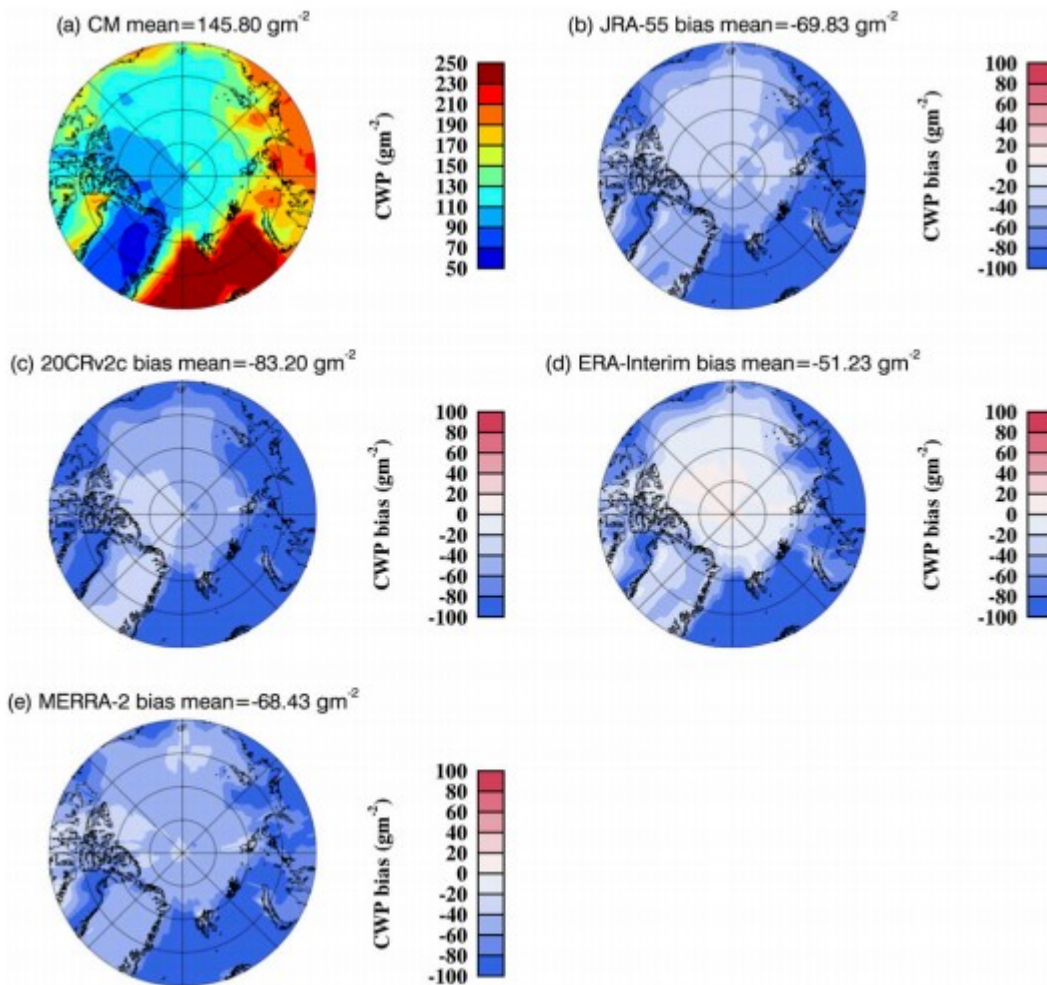


Figure 8 shows the CM-derived CWP during the summer, with an average of 145.8 g m^{-2} over the Arctic, a maximum CWP of about 250 g m^{-2} over the Atlantic Ocean, and a minimum CWP of about 50 g m^{-2} over Greenland. The available four reanalyses show large negative biases over the Atlantic Ocean, Baffin Bay, and coastal regions. The RMSDs of the summer CWP in these four reanalyses are 70.54 , 83.37 , 59.03 , and 69.28 g m^{-2} for JRA-55, 20CRv2c, ERA-Interim, and MERRA-2, respectively (not shown). Therefore, there is a negative offset in each reanalysis, which causes the large CWP bias in the summer.

FIG. 8. As in Fig. 7, but for CWP.



To investigate the impacts of clouds on the TOA and surface radiation budgets, the spatial distributions of the CERES observed and reanalyzed fluxes during the summer are investigated and shown in Figs. 9–11, and the statistics (bias and RMSDs) of all radiative variables are summarized in Tables 3 and 4. During the summer, sunlight is present or almost present for the full 24-h diurnal cycle, and the daily mean solar insolation is nearly invariant with latitude over the Arctic. Therefore, the distribution of all-sky TOA SW_{up} flux is primarily determined by Arctic cloud and aerosol properties, as well as surface albedo. Figure 9a illustrates that the all-sky TOA SW_{up} flux from CERES EBAF increases with latitude over the Arctic excluding Greenland. Note that the North Pole region is still covered by permanent Arctic sea ice during the summer, which may partially contribute to the higher SW_{up} flux at the TOA. The peak in SW_{up} flux over central Greenland is most likely attributed to its higher elevation and surface albedo, as well as much shorter atmospheric path length for solar radiation (Serreze et al. 1998).

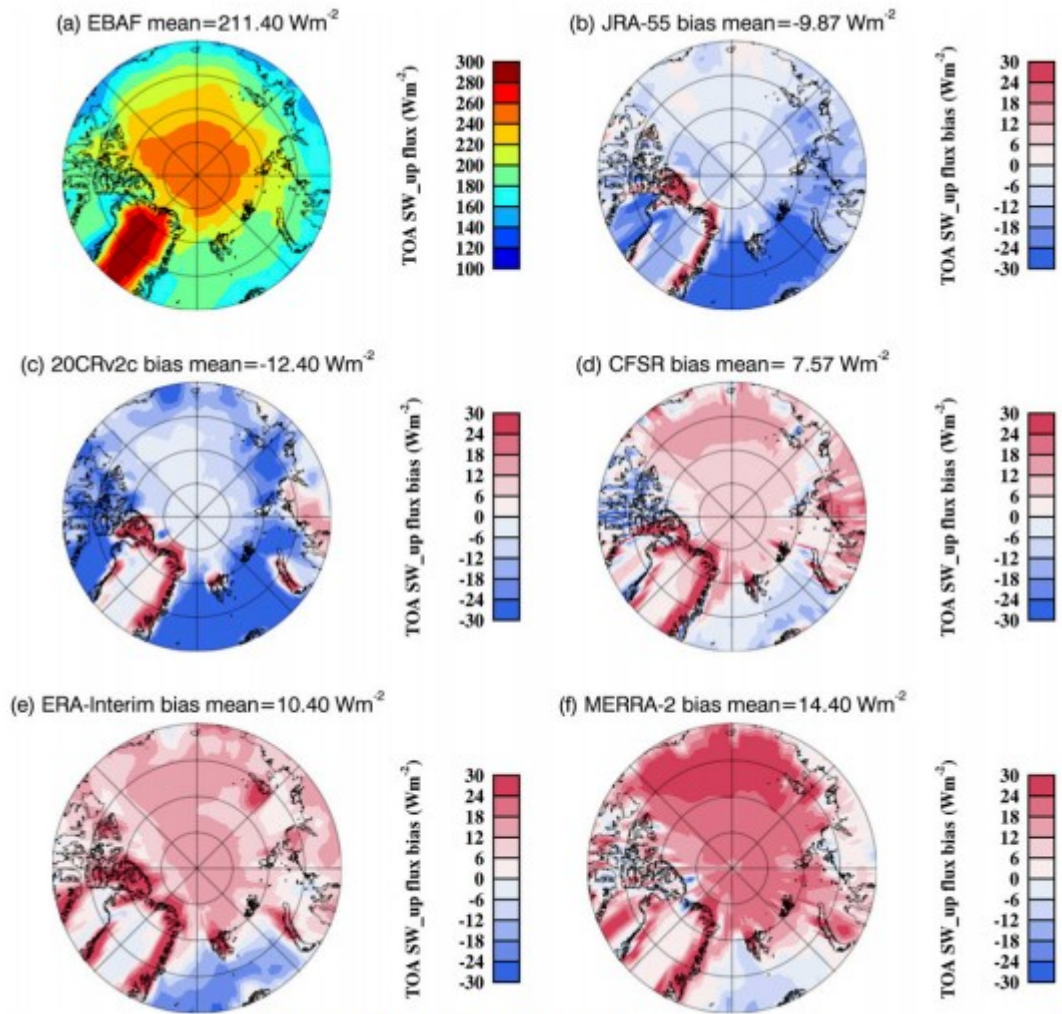


FIG. 9. As in Fig. 7, but for TOA SW_up flux under all-sky conditions.

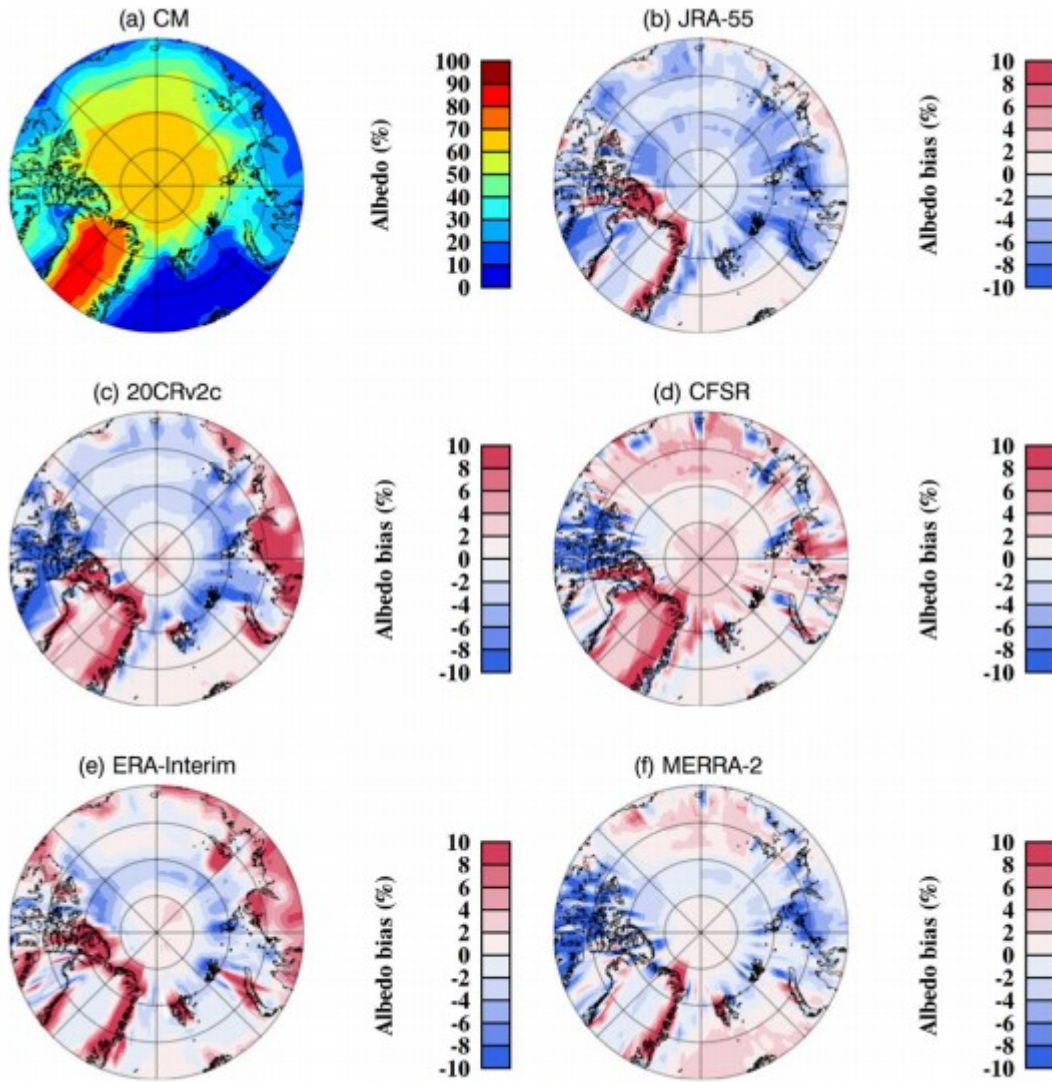


FIG. 10. As in Fig. 7, but for surface albedo.

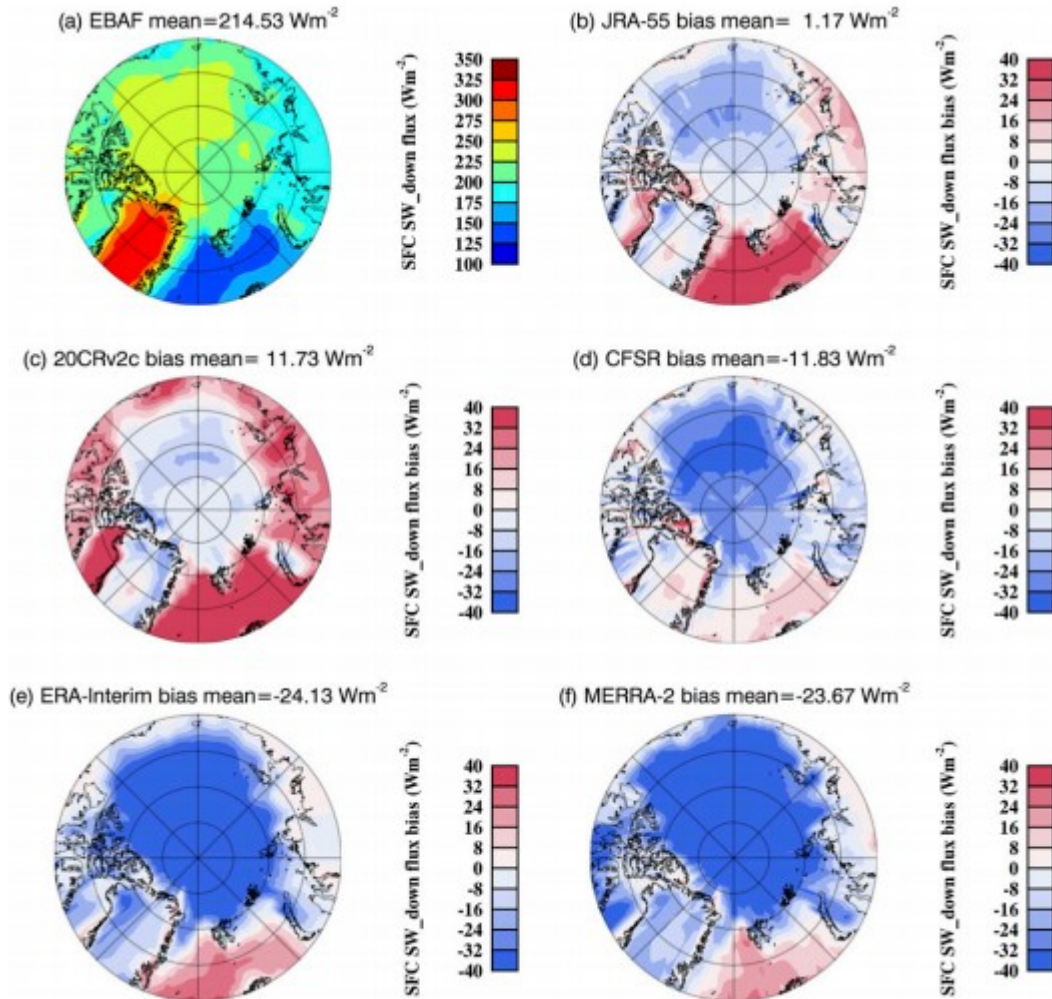


FIG. 11. As in Fig. 7, but for surface SW_down flux.

During summer, the all-sky TOA SW_up fluxes from CFSR, ERA-Interim, and MERRA-2 have positive biases of +7.6, +10.4, and +14.4 $W m^{-2}$, respectively. Most of the positive biases occur over the Arctic Ocean, but with slight negative biases in the Atlantic side of the Arctic Ocean. The spatial distribution of positive bias in MERRA-2 may slightly depend on its CF and surface albedo (Fig. 10) distributions (e.g., Arctic Ocean) but not associated with its CWP. The negative bias in JRA-55 is consistent with its negative biases in CF and CWP over the Atlantic side of the Arctic Ocean, while the negative bias over the Arctic Ocean in 20CRv2c can be better explained by its lower CWP and surface albedo. Interestingly, all five reanalyses show positive biases along the northern and eastern coasts of Greenland, where the elevation is lower and the surface is snow and ice free. The same issue is found in clear-sky condition (not shown). One of the possible reasons to explain this common positive bias is that the changes in surface albedo are not well represented in these reanalyses, as all reanalyses show positive surface albedo biases over this region in Fig. 10.

Reeves Eyre and Zeng (2017) found that the surface elevation fields in many of reanalysis products are smoother than the actual topography of Greenland, as they took 20CR as an example, which has a mostly positive elevation bias around the edge of the ice sheet. This might further contribute to the surface albedo biases. However, English et al. (2014) also pointed out that this problem could be attributed to issues with CERES EBAF clear-sky retrieval algorithm at high latitudes due to low albedo contrasts combined with high-latitude zenith angle. The two clear-sky algorithms based on solar zenith angles suffer from disagreement or errors in high latitudes.

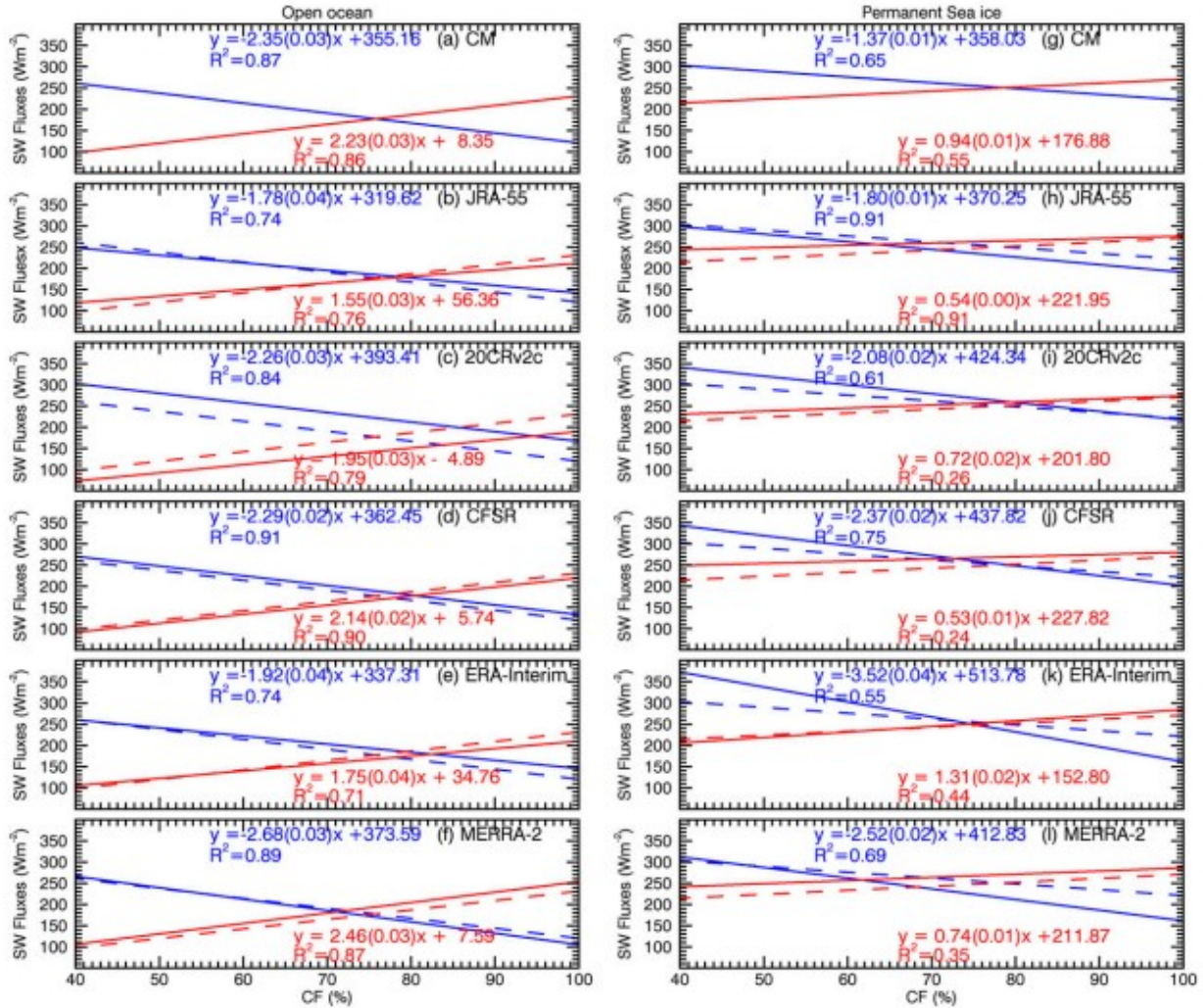
Since the SW_{down} flux at the surface is strongly dependent on CF and CWP (Huang et al. 2017), the spatial distributions of SW_{down} fluxes during the summer are selected and presented in Fig. 11. Collocated with the CF and CWP comparisons in Figs. 7a and 8a, the surface SW_{down} flux from CM has a strong negative correlation with its CF and CWP. For instance, Fig. 11a shows that the lower SW_{down} flux over the North Atlantic Ocean is associated with higher CF and CWP over that region. In addition to CF and CWP, the high surface albedo can offset this cloud-induced attenuation through multiple reflections between the highly reflective surface and clouds (Wendler et al. 1981; Shine 1984; Serreze et al. 1998; Dong et al. 2010). This argument can be further proven by the relatively large SW_{down} flux in the central Arctic Ocean, indicating that cloud attenuation can be partially offset by the multiple reflections between the ice-covered surfaces and clouds in this area.

With the pronounced elevation effect and high surface albedo, as well as low CF and CWP, the maximum surface SW_{down} flux can be found over central Greenland as illustrated in Fig. 11a. CF_{SR}, ERA-Interim, and MERRA-2 are largely negatively biased over the Arctic Ocean. The small negative biases over the land in ERA-Interim and MERRA-2 can be explained by the +8.9 W m⁻² bias in CERES EBAF-surface SW_{down} flux compared to the surface land observations. Additionally, positive biases are found in the North Atlantic Ocean in all five reanalyses. Moreover, surface SW_{down} flux in JRA-55 is relatively consistent with its CF and CWP results.

c. Sensitivity analysis

To quantify the impact of CF (and CWP; not shown) on the TOA and surface radiation budgets, sensitivities of TOA SW_{up} flux and surface SW_{down} flux to CF in July are presented in Fig. 12. The SW fluxes are chosen due to their stronger dependence on cloud properties compared to LW fluxes. Sensitivity studies were also performed for June and August (not shown). Note that these sensitivity studies are conducted over the open ocean (70°–76°N, 0°–46°E) and over permanent sea ice (84°–90°N, all longitudes) because of their different surface albedos.

FIG. 12. Sensitivities of TOA SW_{up} flux (red) and surface SW_{down} flux (blue) to CF based on (a),(g) CERES observations and (b)-(f), (h)-(l) the five selected reanalyses in July over (left) open ocean (70°–76°N, 0°–46°E) and (right) permanent sea ice (84°–90°N, all longitudes) within the Arctic. Regression lines are shown with the σ of the slope in parentheses. The dashed lines are results from CERES to compare with each reanalysis.



In Fig. 12, regression analyses were conducted using all points in July over the two selected regions from both CERES and the five reanalyses. The red lines represent TOA SW_{up} flux, while the blue lines represent SW_{down} flux at the surface. To identify the uncertainty of this regression analysis, the standard error σ of the slope has been determined, as shown in parentheses in each panel of Fig. 12. By calculating the slope $\pm 1.96\sigma$, we obtain the 95% confidence interval. In addition, the coefficient of determination R^2 is also shown with its linear regression.

As shown in Figs. 12a and 12g, CERES-observed TOA SW_{up} fluxes increase from 100 to 230 W m^{-2} as CFs increase from 40% to 100% with a sensitivity of $2.23 \text{ W m}^{-2} \%^{-1}$ over the open ocean (ranging from 1.46 to $2.23 \text{ W m}^{-2} \%^{-1}$ from June to August). Over permanent sea ice, the CERES observed TOA

SW_{up} fluxes increase from 210 to 270 W m⁻² with a sensitivity of 0.94 W m⁻² %⁻¹ (ranging from 0.08 to 0.94 W m⁻² %⁻¹ from June to August) due to the significant contribution from highly reflective sea ice. Among the reanalyses, the slopes of CFSR and MERRA-2 are the closest to the CERES observations over the open ocean with values of 2.14 and 2.46 W m⁻² %⁻¹, respectively. Although the slopes of the reanalyses are closer to the observations over permanent sea ice, the R^2 coefficients are relatively low for both observations and reanalyses compared with those over the open ocean.

The CERES-derived SW_{down} fluxes over the open ocean decrease from 250 to 120 W m⁻² as CFs increase from 40% to 100% with a sensitivity of -2.35 W m⁻² %⁻¹ (ranging from -1.98 to -2.35 W m⁻² %⁻¹ from June to August). Over the permanent sea ice, the SW_{down} fluxes decrease from 300 to 220 W m⁻² with a sensitivity of -1.37 W m⁻² %⁻¹ (ranging from -0.87 to -1.37 W m⁻² %⁻¹ from June to August). The weaker regression slope (less negative) over the permanent sea ice is in part due to multiple reflections of solar radiation between cloud layers and highly reflective surfaces (Dong and Mace 2003). In general, all reanalyzed surface SW_{down} fluxes are more sensitive to CF over permanent sea ice during the summer.

In addition, the R^2 coefficients from the observations indicate that TOA SW_{up} flux and surface SW_{down} flux are not strongly correlated with changes in CWP (not shown). However, all reanalyses tend to overestimate the relationships between TOA SW_{up} flux and CWP, as well as surface SW_{down} flux and CWP for both the open ocean and sea ice except in August. Note that there is a strong dependence between cloud properties and atmospheric state variables such as lower-tropospheric stability and midtropospheric vertical velocity (Barton et al. 2012; Taylor et al. 2015). Therefore, it is possible that these relationships would also vary with different synoptic patterns.

d. Error analysis

To provide insightful suggestions to improve the reanalyses, Table 5 lists various types of error sources quantified in this study. The total errors in reanalysis TOA SW_{up} flux and surface SW_{down} flux can be decomposed into three sources: the error related to the sensitivities of SW flux to CF/CWP ($\epsilon_{\text{sen,CF}}$ and $\epsilon_{\text{sen,CWP}}$), the error due to the reanalysis CF or CWP biases (ϵ_{CF} and ϵ_{CWP}), and the covariance ($\epsilon_{\text{cov,CF}}$ and $\epsilon_{\text{cov,CWP}}$) (Dolinar et al. 2015). The three errors are calculated using following equations:

$$\epsilon_{\text{sen},V} = \left[\left(\frac{\partial \text{SW}}{\partial V} \right)_r - \left(\frac{\partial \text{SW}}{\partial V} \right)_o \right] V_o,$$

$$\epsilon_V = \left(\frac{\partial \text{SW}}{\partial V} \right)_o (V_r - V_o),$$

$$\varepsilon_{\text{cov},V} = \left[\left(\frac{\partial \text{SW}}{\partial V} \right)_r - \left(\frac{\partial \text{SW}}{\partial V} \right)_o \right] (V_r - V_o), \quad \text{and}$$

$$\varepsilon_{\text{total},V} = \varepsilon_{\text{sen},V} + \varepsilon_V + \varepsilon_{\text{cov},V},$$

where SW represents TOA SW_{up} flux or surface SW_{down} flux, and V represents the averaged CF or CWP over the open ocean or permanent sea ice. Subscripts *r* and *o* denote reanalyses and observations, respectively. The slopes derived from sensitivity analysis in Fig. 12 are used for the partial derivative term. Again, we focus on July in this error analysis for two surface types.

TABLE 5. The different error sources in TOA SW_{up} fluxes and surface SW_{down} fluxes over the open ocean and permanent sea ice in July, respectively.

	TOA SW _{up} fluxes (W m ⁻²)				Surface SW _{down} fluxes (W m ⁻²)			
	JRA-55	20CRv2c	ERA-Interim	MERRA-2	JRA-55	20CRv2c	ERA-Interim	MERRA-2
Cloud fraction								
Sensitivity error								
Open sea	-59.43	-24.47	-41.95	20.10	49.81	7.87	37.58	-28.84
Sea ice	-32.06	-17.63	29.66	-16.03	-34.47	-56.91	-172.34	-92.18
CF biases								
Open sea	-34.29	-27.89	-7.49	-23.14	36.13	29.39	7.89	24.38
Sea ice	-4.92	8.30	14.17	2.80	7.17	-12.09	-20.65	-4.08
Covariances								
Open sea	10.46	3.50	1.61	-2.39	-8.76	-1.13	-1.44	3.42
Sea ice	2.09	-1.94	5.58	-0.60	2.25	-6.27	-32.41	-3.42
Total								
Open sea	-83.26	-48.86	-47.83	-5.42	77.19	36.13	44.03	-1.03
Sea ice	-34.89	-11.29	49.41	-13.83	-25.05	-75.27	-225.40	-99.68
Cloud water path								
Sensitivity error								
Open sea	98.03	267.35	115.85	145.56	-136.64	-323.79	-139.62	-169.32
Sea ice	16.65	25.53	19.98	41.07	-65.49	-109.89	-53.28	-105.45
CWP biases								
Open sea	-29.62	-34.86	-28.10	-28.69	27.64	32.54	26.23	26.78
Sea ice	-2.53	-3.23	0.65	-4.22	7.02	8.97	-1.82	11.74
Covariances								
Open sea	-65.16	-209.16	-73.06	-93.72	90.83	253.33	88.04	109.03
Sea ice	-4.21	-8.25	1.31	-17.38	16.56	35.51	-3.49	44.62
Total								
Open sea	3.25	23.32	14.69	23.14	-18.17	-37.93	-25.34	-33.52
Sea ice	9.91	14.05	21.94	19.47	-41.91	-48.86	-58.59	-49.09

As listed in Table 5, the most dominant error source in each reanalysis is the sensitivity error for both TOA SW_{up} flux and surface SW_{down} flux. Over the open ocean, the sensitivity error of CWP contributes more than that of CF in all reanalyses, which is consistent with the findings in section 3c. Similarly, the CWP sensitivity error is found to be the dominant error source over permanent sea ice in all reanalyses excluding the ERA-Interim. The ERA-Interim product significantly overestimates the sensitivities of TOA SW_{up} flux and surface SW_{down} flux to CF over permanent sea ice as shown in Fig. 10, which makes CF sensitivity error the largest term.

Moreover, the correlations and standard deviations (normalized by observations) between the reanalyses and CERES observations in terms of

CF, CWP, and TOA and surface SW and LW radiative fluxes during the summer are summarized in Table 6. These values are calculated by using all points in spatial and temporal scales from 2000 to 2012. Generally, all reanalyses have the lowest correlations in CWP and CF, ranging from 0.23 to 0.67, but correlations are much higher in TOA and surface radiative fluxes. These results indicate that all five selected reanalyses can better predict the TOA and surface radiative fluxes but have some challenges when simulating Arctic cloud properties. In general, MERRA-2 and JRA-55 exhibit comparatively higher correlations to observations for Arctic cloud and radiation properties.

TABLE 6. The correlation and standard deviation (normalized by CERES–MODIS observations) in each reanalysis over the Arctic during the summer (standard deviations are shown in parentheses).

Variables	JRA-55	20CRv2c	CFSR	ERA-Interim	MERRA-2
CF	0.678 (0.139)	0.524 (0.144)	0.662 (0.151)	0.653 (0.151)	0.670 (0.136)
CWP	0.507 (0.399)	0.229 (0.449)	—	0.328 (0.450)	0.625 (0.367)
TOA SW _{all} [↑]	0.916 (0.111)	0.913 (0.116)	0.937 (0.097)	0.945 (0.090)	0.967 (0.074)
TOA SW _{clr} [↑]	0.919 (0.170)	—	0.929 (0.164)	0.947 (0.138)	0.955 (0.150)
TOA LW _{all} [↑]	0.916 (0.012)	0.750 (0.020)	0.906 (0.013)	0.949 (0.010)	0.898 (0.014)
TOA LW _{clr} [↑]	0.816 (0.021)	—	0.831 (0.020)	0.812 (0.021)	0.820 (0.020)
Surface SW _{all} [↑]	0.926 (0.254)	0.939 (0.226)	0.932 (0.236)	0.913 (0.266)	0.952 (0.200)
Surface SW _{clr} [↑]	0.951 (0.106)	0.931 (0.123)	0.949 (0.106)	0.904 (0.146)	0.936 (0.117)
Surface LW _{all} [↑]	0.898 (0.026)	0.852 (0.030)	—	0.882 (0.027)	0.885 (0.027)
Surface LW _{clr} [↑]	0.910 (0.033)	0.847 (0.041)	0.892 (0.037)	0.834 (0.046)	0.887 (0.037)

4. Summary and conclusions

This study has compared the reanalysis cloud and radiation properties from five selected reanalyses with the NASA CERES-derived CFs, CWPs, TOA and surface radiative fluxes in the Arctic region over the period of March 2000–February 2012 and 4-yr CC-derived CFs. From these comprehensive comparisons, we draw the following key conclusions and provide insightful suggestions for model improvement:

1. The monthly mean CFs in all reanalyses, except JRA-55, are close to or slightly higher than CC-derived CFs from May to September, but from about a few percentages to 20% higher over the period of October–April. Compared to CC, CM-derived CFs have a negative bias of -11.2% in the annual mean, with almost identical values in summer, but wintertime CF cannot be confidently evaluated until instrument simulators are implemented in reanalysis products. Although the reanalyzed CWPs generally follow the seasonal variations of CM, their annual means are only half or even less than the observations (126 g m^{-2}). The differences in TOA SW_{up} flux between CERES EBAF and the reanalyses range from -6.5 W m^{-2} in JRA-55 to $+3.9 \text{ W m}^{-2}$ in MERRA-2 compared to the observed annual average of 99.6 W m^{-2} . The annual mean differences in TOA LW_{up} flux range from -5.2 W m^{-2} in 20CRv2c to $+6.1 \text{ W m}^{-2}$ in JRA-55. As for the surface SW and LW flux comparisons, the annual mean differences between CERES EBAF and reanalyses are less than 16 W m^{-2} .

2. Although their Arctic domain averaged summer means are nearly identical, CM-derived CFs are approximately 6%–10% higher over the Ocean and 10% lower over Greenland compared to CC values during the 4-yr period. Compared to CM, 20CRv2c, CFSR, and ERA-Interim exhibit slight positive biases over the Arctic Ocean. CFSR, MERRA-2, and especially JRA-55 underestimate CF over Greenland if we take the CM uncertainty into account. All reanalyses exhibit large negative biases of CWP in summer, presumably due to a negative offset across entire Arctic.
3. The spatial distribution comparison shows that all reanalyses show positive biases along the northern and eastern coasts of Greenland, which may be attributed to model elevation biases or issues with the CERES EBAF clear-sky retrieval algorithm at high latitudes.
4. The most dominant source of error in each reanalysis is the sensitivity error for both TOA SW_{up} flux and surface SW_{down} flux. The sensitivity of surface SW_{down} flux to CF over permanent sea ice is overestimated in each reanalysis for all three summer months. Moreover, all reanalyses tend to overestimate the relationships between TOA SW_{up} flux/surface SW_{down} flux and CWP, as they do not exhibit strong correlations to the observations.
5. All reanalyses have the low correlations in CWP and CF with respect to CM-derived cloud properties, ranging from 0.23 to 0.67, but the correlations in TOA and surface radiative fluxes are much higher. These results indicate that all five selected reanalyses can better predict radiative fluxes but have some challenges when simulating Arctic cloud properties. In general, JRA-55 does a good job in terms of physical consistency of cloud and radiation variables. MERRA-2 and JRA-55 exhibit comparatively higher correlations to observations for Arctic cloud and radiation properties.

We understand that the cloud comparison between reanalysis and satellite observations may be unfair given the lack of simulator technique in current global reanalysis. A more reasonable evaluation can be made when COSP is fully applied in the reanalysis products. Another limitation of this study is that the uncertainties of CM-derived surface radiative fluxes have not been well quantified over the Arctic Ocean. De Boer et al. (2014) used Arctic Summer Cloud Ocean Study (ASCOS) drifting base camp data to evaluate various global reanalysis and model results, and concluded that ERA-Interim outperforms other models in representing surface energy budget terms. A thorough evaluation for both satellite and reanalysis products can be done with more and more recent Arctic Ocean field campaign datasets available.

In addition to CF and CWP, other cloud properties such as cloud type, height, and cloud microphysical and optical properties may affect both TOA and surface radiation fluxes. The reanalyzed aerosols and land and ocean properties can also be examined to investigate the radiation budget biases.

Furthermore, the Arctic sea ice coverage also plays an essential role in determining both TOA and surface radiation budgets. Reanalyses usually use a mix of data sources for sea ice concentrations (Table 2). CFSR is the only product with a modeled sea ice thickness. According to Lindsay et al. (2014), the sea ice differences are minor in various reanalyses, although the ice extent is specified by using different sources. Therefore, we believe that sea ice is not an important source of error that contributes to simulated Arctic radiation properties. In the future, we would like to focus on the sea ice-cloud-radiation feedback to extend this study.

This study reports on the performance of reanalyzed Arctic cloud fractions and their effects on the TOA and surface radiation budgets. The results presented in this study provide useful information for modelers to improve their cloud and radiation parameterizations over the Arctic, as well as to guide potential users to choose proper reanalysis datasets in different situations. In addition, this study hopefully offers motivation for further investigations of Arctic climate variability based on these selected reanalyses.

Acknowledgments

This study was supported by NOAA MAPP Grant under NA13OAR4310105 at the University of North Dakota and NASA CERES project under Grant NNX17AC52G at The University of Arizona. NASA CERES-MODIS SYN1deg, EBAF-TOA and EBAF-surface products are available at <http://ceres.larc.nasa.gov/>. The BSRN dataset can be accessed from World Radiation Monitoring Center at <http://www.bsrn.awi.de/>. The various reanalysis datasets are available at reanalyses.org. Also, we thank Jack Reeves Eyre for the discussion and three anonymous reviewers for their suggestions.

REFERENCES

- Bacmeister, J. T., M. J. Suarez, and F. R. Robertson, 2006: Rain reevaporation, boundary layer-convection interactions, and Pacific rainfall patterns in an AGCM. *J. Atmos. Sci.*, 63, 3383–3403, doi:<https://doi.org/10.1175/JAS3791.1>.
- Barton, N. P., S. A. Klein, J. S. Boyle, and Y. Y. Zhang, 2012: Arctic synoptic regimes: Comparing domain-wide Arctic cloud observations with CAM4 and CAM5 during similar dynamics. *J. Geophys. Res.*, 117, D15205, doi:<https://doi.org/10.1029/2012JD017589>.
- Bodas-Salcedo, A., and Coauthors, 2011: COSP: Satellite simulation software for model assessment. *Bull. Amer. Meteor. Soc.*, 92, 1023–1043, doi:<https://doi.org/10.1175/2011BAMS2856.1>.
- Boeke, R. C., and P. C. Taylor, 2016: Evaluation of the Arctic surface radiation budget in CMIP5 models. *J. Geophys. Res. Atmos.*, 121, 8525–8548, doi:<https://doi.org/10.1002/2016JD025099>.

Bosilovich, M., and Coauthors, 2015: MERRA-2: Initial evaluation of climate. NASA Tech. Memo. NASA/TM-2015-104606/Vol. 43, 145 pp., <https://gmao.gsfc.nasa.gov/pubs/docs/Bosilovich803.pdf>.

Bromwich, D. H., and S. H. Wang, 2005: Evaluation of the NCEP-NCAR and ECMWF 15- and 40-yr reanalyses using rawinsonde data from two independent Arctic field experiments. *Mon. Wea. Rev.*, 133, 3562–3578, doi:<https://doi.org/10.1175/MWR3043.1>.

Bromwich, D. H., R. I. Cullather, and M. C. Serreze, 2000: Reanalyses depictions of the Arctic atmospheric moisture budget. *The Freshwater Budget of the Arctic Ocean*, E. Lewis et al., Eds., NATO Science Series, Vol. 70, Springer, 163–196, doi:https://doi.org/10.1007/978-94-011-4132-1_8.

Bromwich, D. H., S.-H. Wang, and A. J. Monaghan, 2002: ERA-40 representation of the Arctic atmospheric moisture budget. *ECMWF Workshop on Re-Analysis*, Reading, United Kingdom, ECMWF, 287–298.

Bromwich, D. H., R. L. Fogt, K. I. Hodges, and J. E. Walsh, 2007: A tropospheric assessment of the ERA-40, NCEP, and JRA-25 global reanalyses in the polar regions. *J. Geophys. Res.*, 112, D10111, doi:<https://doi.org/10.1029/2006JD007859>.

CERES, 2014: CERES_EBAF_Ed2.8 Data Quality Summary. 46 pp. [Available online at http://ceres.larc.nasa.gov/documents/DQ_summaries/CERES_EBAF_Ed2.8_DQS.pdf.]

CERES, 2015: CERES_EBAF-Surface_Ed2.8 Data Quality Summary. CERES Rep., 42 pp. [Available online at http://ceres.larc.nasa.gov/documents/DQ_summaries/CERES_EBAF-Surface_Ed2.8_DQS.pdf.]

Chou, M. D., and M. J. Suarez, 1999: A solar radiation parameterization for atmospheric studies. NASA Tech. Memo. NASA/TM-1999-104606, Vol. 15, 51 pp. [Available online at <https://ntrs.nasa.gov/search.jsp?R=19990060930>.]

Chou, M. D., M. J. Suarez, C.-H. Ho, M. M.-H. Yan, and K.-T. Lee, 1998: Parameterizations for cloud overlapping and shortwave single-scattering properties for use in general circulation and cloud ensemble models. *J. Climate*, 11, 202–214, doi:[https://doi.org/10.1175/1520-0442\(1998\)011<0202:PFCOAS>2.0.CO;2](https://doi.org/10.1175/1520-0442(1998)011<0202:PFCOAS>2.0.CO;2).

Chou, M. D., M. J. Suarez, X.-Z. Liang, and M. M.-H. Yan, 2001: A thermal infrared radiation parameterization for atmospheric studies. NASA Tech. Memo. NASA/TM-2001-104606, Vol. 19, 56 pp. [Available online at <https://ntrs.nasa.gov/search.jsp?R=20010072848>.]

Christensen, M. W., A. Behrangi, T. S. L'Ecuyer, N. B. Wood, M. D. Lebsock, and G. L. Stephens, 2016: Arctic observation and reanalysis integrated system: A new data product for validation and climate study. *Bull. Amer. Meteor. Soc.*, 97, 907–916, doi:<https://doi.org/10.1175/BAMS-D-14-00273.1>.

- Compo, G. P., and Coauthors, 2011: The Twentieth Century Reanalysis Project. *Quart. J. Roy. Meteor. Soc.*, 137, 1–28, doi:<https://doi.org/10.1002/qj.776>.
- Curry, J. A., J. L. Schramm, W. B. Rossow, and D. Randall, 1996: Overview of Arctic cloud and radiation characteristics. *J. Climate*, 9, 1731–1764, doi:[https://doi.org/10.1175/1520-0442\(1996\)009<1731:OOACAR>2.0.CO;2](https://doi.org/10.1175/1520-0442(1996)009<1731:OOACAR>2.0.CO;2).
- De Boer, G., and Coauthors, 2014: Near-surface meteorology during the Arctic Summer Cloud Ocean Study (ASCOS): Evaluation of reanalyses and global climate models. *Atmos. Chem. Phys.*, 14, 427–445, doi:<https://doi.org/10.5194/acp-14-427-2014>.
- Dee, D. P., and Coauthors, 2011: The ERA-Interim reanalysis: Configuration and performance of the data assimilation system. *Quart. J. Roy. Meteor. Soc.*, 137, 553–597, doi:<https://doi.org/10.1002/qj.828>.
- Deng, M., G. G. Mace, Z. Wang, and E. Berry, 2015: *CloudSat* 2C-ICE product update with a new Z_e parameterization in lidar-only region. *J. Geophys. Res. Atmos.*, 120, 12 198–12 208, doi:<https://doi.org/10.1002/2015JD023600>.
- Dolinar, E. K., X. Dong, B. Xi, J. H. Jiang, and H. Su, 2015: Evaluation of CMIP5 simulated clouds and TOA radiation budgets using NASA satellite observations. *Climate Dyn.*, 44, 2229–2247, doi:<https://doi.org/10.1007/s00382-014-2158-9>.
- Dong, X., and G. G. Mace, 2003: Arctic stratus cloud properties and radiative forcing derived from ground-based data collected at Barrow, Alaska. *J. Climate*, 16, 445–461, doi:[https://doi.org/10.1175/1520-0442\(2003\)016<0445:ASCPAR>2.0.CO;2](https://doi.org/10.1175/1520-0442(2003)016<0445:ASCPAR>2.0.CO;2).
- Dong, X., B. Xi, K. Crosby, and P. Minnis, 2006: A climatology of midlatitude continental clouds from the ARM SGP Central Facility. Part II: Cloud fraction and surface radiative forcing. *J. Climate*, 19, 1765–1783, doi:<https://doi.org/10.1175/JCLI3710.1>.
- Dong, X., P. Minnis, B. Xi, S. Sun-Mack, and Y. Chen, 2008: Comparison of CERES-MODIS stratus cloud properties with ground-based measurements at the DOE ARM Southern Great Plains site. *J. Geophys. Res.*, 113, D03204, doi:<https://doi.org/10.1029/2007JD008438>.
- Dong, X., B. Xi, K. Crosby, C. N. Long, R. S. Stone, and M. D. Shupe, 2010: A 10 year climatology of Arctic cloud fraction and radiative forcing at Barrow, Alaska. *J. Geophys. Res.*, 115, D17212, doi:<https://doi.org/10.1029/2009JD013489>.
- Dong, X., B. Xi, K. Crosby, S. Qiu, P. Minnis, S. Sun-Mack, and F. Rose, 2016: A radiation closure study of Arctic cloud microphysical properties using the collocated satellite-surface data and Fu-Liou radiative transfer model. *J. Geophys. Res. Atmos.*, 121, 10 175–10 198, doi:<https://doi.org/10.1002/2016JD025255>.

Ebert, E. E., and J. A. Curry, 1993: An intermediate one-dimensional thermodynamic sea ice model for investigating ice-atmosphere interactions. *J. Geophys. Res.*, 98, 10 085–10 109, doi:<https://doi.org/10.1029/93JC00656>.

English, J. M., J. E. Kay, A. Gettelman, X. Liu, Y. Wang, Y. Zhang, and H. Chepfer, 2014: Contributions of clouds, surface albedos, and mixed-phase ice nucleation schemes to Arctic radiation biases in CAM5. *J. Climate*, 27, 5174–5197, doi:<https://doi.org/10.1175/JCLI-D-13-00608.1>.

English, J. M., A. Gettelman, and G. R. Henderson, 2015: Arctic radiative fluxes: Present-day biases and future projections in CMIP5 models. *J. Climate*, 28, 6019–6038, doi:<https://doi.org/10.1175/JCLI-D-14-00801.1>.

ECMWF, 2014: IFS Documentation-Cy40r1 Part IV: Physical processes. ECMWF, 190 pp. [Available online at https://www.ecmwf.int/sites/default/files/IFS_CY40R1_Part4.pdf.]

Fels, S. B., and M. D. Schwarzkopf, 1975: The simplified exchange approximation: A new method for radiative transfer calculations. *J. Atmos. Sci.*, 32, 1475–1488, doi:[https://doi.org/10.1175/1520-0469\(1975\)032<1475:TSEAAAN>2.0.CO;2](https://doi.org/10.1175/1520-0469(1975)032<1475:TSEAAAN>2.0.CO;2).

Gorodetskaya, I. V., and L. B. Tremblay, 2008: Arctic cloud properties and radiative forcing from observations and their role in sea ice decline predicted by the NCAR CCSM3 Model during the 21st century. *Arctic Sea Ice Decline: Observations, Projections, Mechanisms, and Implications, Geophys. Monogr.*, Vol. 180, Amer. Geophys. Union, 47–62, doi:<https://doi.org/10.1029/180GM05>.

Halliwel, D., 2012: Basic and other measurements of radiation at station Alert (2004–2008). AeroCan, Wilcox, PANGAEA, accessed 10 May 2016, doi:<https://doi.org/10.1594/PANGAEA.788590>.

Hirahara, S., M. Ishii, and Y. Fukuda, 2014: Centennial-scale sea surface temperature analysis and its uncertainty. *J. Climate*, 27, 57–75, doi:<https://doi.org/10.1175/JCLI-D-12-00837.1>.

Hou, Y., K. Campana, and S. Yang, 1996: Shortwave radiation calculations in the NCEP's global model. *Proc. Int. Radiation Symp. 1996*, Fairbanks, AK, IRS, 19–24.

Hou, Y., S. Moorthi, K. Campana, 2002: Parameterization of solar radiation transfer in the NCEP models. NCEP Office Note 441, 46 pp.

Huang, Y., X. Dong, B. Xi, E. K. Dolinar, and R. E. Stanfield, 2017: The footprints of 16 year trends of Arctic springtime cloud and radiation properties on September sea ice retreat. *J. Geophys. Res. Atmos.*, 122, 2179–2193, doi:<https://doi.org/10.1002/2016JD026020>.

IPCC, 2013: *Climate Change 2013: The Physical Science Basis*. Cambridge University Press, 1535 pp.

JMA, 2013: Outline of the operational numerical weather prediction at the Japan Meteorological Agency. JMA. [Available online at <http://www.jma.go.jp/jma/jma-eng/jma-center/nwp/outline2013-nwp/index.htm>.]

Karlsson, J., and G. Svensson, 2011: The simulation of Arctic clouds and their influence on the winter surface temperature in present-day climate in the CMIP3 multi-model dataset. *Climate Dyn.*, 36, 623–635, doi:<https://doi.org/10.1007/s00382-010-0758-6>.

Kato, S., S. Sun-Mack, W. F. Miller, F. G. Rose, Y. Chen, P. Minnis, and B. A. Wielicki, 2010: Relationships among cloud occurrence frequency, overlap, and effective thickness derived from *CALIPSO* and *CloudSat* merged cloud vertical profiles. *J. Geophys. Res.*, 115, D00H28, doi:<https://doi.org/10.1029/2009JD012277>.

Kato, S., N. G. Loeb, F. G. Rose, D. R. Doelling, D. A. Rutan, T. E. Caldwell, L. Yu, and R. A. Weller, 2013: Surface irradiances consistent with CERES-derived top-of-atmosphere shortwave and longwave irradiances. *J. Climate*, 26, 2719–2740, doi:<https://doi.org/10.1175/JCLI-D-12-00436.1>.

Kay, J. E., and T. L'Ecuyer, 2013: Observational constraints on Arctic Ocean clouds and radiative fluxes during the early 21st century. *J. Geophys. Res. Atmos.*, 118, 7219–7236, doi:<https://doi.org/10.1002/jgrd.50489>.

Kobayashi, S., and Coauthors, 2015: The JRA-55 Reanalysis: General specifications and basic characteristics. *J. Meteor. Soc. Japan*, 93, 5–48, doi:<https://doi.org/10.2151/jmsj.2015-001>.

Komurcu, M., and Coauthors, 2014: Intercomparison of the cloud water phase among global climate models. *J. Geophys. Res. Atmos.*, 119, 3372–3400, doi:<https://doi.org/10.1002/2013JD021119>.

Lindsay, R., M. Wensnahan, A. Schweiger, and J. Zhang, 2014: Evaluation of seven different atmospheric reanalysis products in the Arctic. *J. Climate*, 27, 2588–2606, doi:<https://doi.org/10.1175/JCLI-D-13-00014.1>.

Liu, Y., and J. R. Key, 2016: Assessment of Arctic cloud cover anomalies in atmospheric reanalysis products using satellite data. *J. Climate*, 29, 6065–6083, doi:<https://doi.org/10.1175/JCLI-D-15-0861.1>.

Loeb, N. G., B. A. Wielicki, D. R. Doelling, G. L. Smith, D. F. Keyes, S. Kato, N. Manalo-Smith, and T. Wong, 2009: Toward optimal closure of the Earth's top-of-atmosphere radiation budget. *J. Climate*, 22, 748–766, doi:<https://doi.org/10.1175/2008JCLI2637.1>.

Mace, G. G., Y. Zhang, S. Platnick, M. D. King, P. Minnis, and P. Yang, 2005: Evaluation of cirrus cloud properties from MODIS radiances using cloud properties derived from ground-based data collected at the ARM SGP site. *J. Appl. Meteor.*, 44, 221–240, doi:<https://doi.org/10.1175/JAM2193.1>.

Minnis, P., D. F. Young, B. A. Wielicki, P. W. Heck, X. Dong, L. L. Stowe, and R. M. Welch, 1999: CERES cloud properties derived from multispectral VIRS data. *Satellite Remote Sensing of Clouds and the Atmosphere IV*, J. E. Russell, Ed., International Society for Optics and Photonics (SPIE Proceedings, Vol. 3867), doi:<https://doi.org/10.1117/12.373047>.

Minnis, P., D. F. Young, B. A. Wielicki, S. Sun-Mack, Q. Z. Trepte, Y. Chen, P. W. Heck, and X. Dong, 2002: A global cloud database from VIRS and MODIS for CERES. *Optical Remote Sensing of the Atmosphere and Clouds III*, H.-L. Huang et al., Eds., International Society for Optics and Photonics (SPIE Proceedings, Vol. 4891), doi:<https://doi.org/10.1117/12.467317>.

Minnis, P., and Coauthors, 2008: Cloud detection in nonpolar regions for CERES using TRMM VIRS and *Terra* and *Aqua* MODIS data. *IEEE Trans. Geosci. Remote Sens.*, 46, 3857–3884, doi:<https://doi.org/10.1109/TGRS.2008.2001351>.

Minnis, P., and Coauthors, 2011a: CERES edition-2 cloud property retrievals using TRMM VIRS and *Terra* and *Aqua* MODIS data—Part I: Algorithms. *IEEE Trans. Geosci. Remote Sens.*, 49, 4374–4400, doi:<https://doi.org/10.1109/TGRS.2011.2144601>.

Minnis, P., and Coauthors, 2011b: CERES edition-2 cloud property retrievals using TRMM VIRS and *Terra* and *Aqua* MODIS data—Part II: Examples of average results and comparisons with other data. *IEEE Trans. Geosci. Remote Sens.*, 49, 4401–4430, doi:<https://doi.org/10.1109/TGRS.2011.2144602>.

Mlawer, E. J., S. J. Taubman, P. D. Brown, M. J. Iacono, and S. A. Clough, 1997: Radiative transfer for inhomogeneous atmospheres: RRTM, a validated correlated-*k* model for the longwave. *J. Geophys. Res.*, 102, 16 663–16 682, doi:<https://doi.org/10.1029/97JD00237>.

Moorthi, S., H. L. Pan, and P. Caplan, 2001: Changes to the 2001 NCEP operational MRF/AVN global analysis/forecast system. NWS Tech. Procedures Bull. 484, 14 pp. [Available online at <http://www.nws.noaa.gov/om/tpb/484.pdf>.]

NCAR, 2015: The Climate Data Guide: NOAA 20th-Century Reanalysis, version 2 and 2c. NCAR, accessed 12 June 2016. [Available online at <https://climatedataguide.ucar.edu/climate-data/noaa-20th-century-reanalysis-version-2-and-2c>.]

Ohmura, A., and Coauthors, 1998: Baseline Surface Radiation Network (BSRN/WCRP): New precision radiometry for climate research. *Bull. Amer. Meteor. Soc.*, 79, 2115–2136, doi:[https://doi.org/10.1175/1520-0477\(1998\)079<2115:BSRNBW>2.0.CO;2](https://doi.org/10.1175/1520-0477(1998)079<2115:BSRNBW>2.0.CO;2).

Reeves Eyre, J. E. J., and X. Zeng, 2017: Evaluation of Greenland near surface air temperature datasets. *Cryosphere*, 11, 1591–1605, doi:<https://doi.org/10.5194/tc-11-1591-2017>.

Rienecker, M. M., and Coauthors, 2011: MERRA: NASA's Modern-Era Retrospective Analysis for Research and Applications. *J. Climate*, 24, 3624–3648, doi:<https://doi.org/10.1175/JCLI-D-11-00015.1>.

Rutan, D. A., F. G. Rose, N. M. Smith, and T. P. Charlock, 2001: Validation data set for CERES surface and atmospheric radiation budget (SARB). *GEWEX News*, No. 11 (1), International GEWEX Project Office, Silver Spring, MD, 11–12.

Saha, S., and Coauthors, 2006: The NCEP Climate Forecast System. *J. Climate*, 19, 3483–3517, doi:<https://doi.org/10.1175/JCLI3812.1>.

Saha, S., and Coauthors, 2010: The NCEP Climate Forecast System Reanalysis. *Bull. Amer. Meteor. Soc.*, 91, 1015–1057, doi:<https://doi.org/10.1175/2010BAMS3001.1>.

Saha, S., and Coauthors, 2014: The NCEP Climate Forecast System version 2. *J. Climate*, 27, 2185–2208, doi:<https://doi.org/10.1175/JCLI-D-12-00823.1>.

Schwarzkopf, M. D., and S. B. Fels, 1991: The simplified exchange method revisited: An accurate, rapid method for computation of infrared cooling rates and fluxes. *J. Geophys. Res.*, 96, 9075–9096, doi:<https://doi.org/10.1029/89JD01598>.

Serreze, M. C., and C. M. Hurst, 2000: Representation of mean Arctic precipitation from NCEP–NCAR and ERA Reanalyses. *J. Climate*, 13, 182–201, doi:[https://doi.org/10.1175/1520-0442\(2000\)013<0182:ROMAPF>2.0.CO;2](https://doi.org/10.1175/1520-0442(2000)013<0182:ROMAPF>2.0.CO;2).

Serreze, M. C., J. R. Key, J. E. Box, J. A. Maslanik, and K. Steffen, 1998: A new monthly climatology of global radiation for the Arctic and comparisons with NCEP–NCAR reanalysis and ISCCP–C2 fields. *J. Climate*, 11, 121–136, doi:[https://doi.org/10.1175/1520-0442\(1998\)011<0121:ANMCOG>2.0.CO;2](https://doi.org/10.1175/1520-0442(1998)011<0121:ANMCOG>2.0.CO;2).

Shine, K. P., 1984: Parametrization of the shortwave flux over high albedo surfaces as a function of cloud thickness and surface albedo. *Quart. J. Roy. Meteor. Soc.*, 110, 747–764, doi:<https://doi.org/10.1002/qj.49711046511>.

Shupe, M. D., and J. M. Intrieri, 2004: Cloud radiative forcing of the Arctic surface: The influence of cloud properties, surface albedo, and solar zenith angle. *J. Climate*, 17, 616–628, doi:[https://doi.org/10.1175/1520-0442\(2004\)017<0616:CRFOTA>2.0.CO;2](https://doi.org/10.1175/1520-0442(2004)017<0616:CRFOTA>2.0.CO;2).

Sommeria, G., and J. W. Deardorff, 1977: Subgrid-scale condensation in models of nonprecipitating clouds. *J. Atmos. Sci.*, 34, 344–355, doi:[https://doi.org/10.1175/1520-0469\(1977\)034<0344:SSCIMO>2.0.CO;2](https://doi.org/10.1175/1520-0469(1977)034<0344:SSCIMO>2.0.CO;2).

Stanfield, R. E., X. Dong, B. Xi, A. Kennedy, A. D. Del Genio, P. Minnis, and J. H. Jiang, 2014: Assessment of NASA GISS CMIP5 and post-CMIP5 simulated clouds and TOA radiation budgets using satellite observations. Part I: Cloud fraction and properties. *J. Climate*, 27, 4189–4208, doi:<https://doi.org/10.1175/JCLI-D-13-00558.1>.

- Stubenrauch, C. J., and Coauthors, 2013: Assessment of global cloud datasets from satellites: Project and database initiated by the GEWEX Radiation Panel. *Bull. Amer. Meteor. Soc.*, 94, 1031–1049, doi:<https://doi.org/10.1175/BAMS-D-12-00117.1>.
- Taylor, P. C., S. Kato, K.-M. Xu, and M. Cai, 2015: Covariance between Arctic sea ice and clouds within atmospheric state regimes at the satellite footprint level. *J. Geophys. Res. Atmos.*, 120, 12 656–12 678, doi:<https://doi.org/10.1002/2015JD023520>.
- Tiedtke, M., 1993: Representation of clouds in large-scale models. *Mon. Wea. Rev.*, 121, 3040–3061, doi:[https://doi.org/10.1175/1520-0493\(1993\)121<3040:ROCILS>2.0.CO;2](https://doi.org/10.1175/1520-0493(1993)121<3040:ROCILS>2.0.CO;2).
- Van den Dool, H. M., 2011: Reconstruction of the solar constant back to 1750. NCEP CPC, 4 pp., http://webcache.googleusercontent.com/search?q=cache:4RjDcSffpoMj:www.cpc.ncep.noaa.gov/products/people/wd51hd/vddoolpubs/other/other_solar_reconstruction.doc+&cd=3&hl=en&ct=clnk&gl=us.
- Waliser, D. E., and Coauthors, 2009: Cloud ice: A climate model challenge with signs and expectations of progress. *J. Geophys. Res.*, 114, D00A21, doi:<https://doi.org/10.1029/2008JD010015>.
- Walsh, J. E., W. L. Chapman, and D. H. Portis, 2009: Arctic cloud fraction and radiative fluxes in atmospheric reanalyses. *J. Climate*, 22, 2316–2334, doi:<https://doi.org/10.1175/2008JCLI2213.1>.
- Wang, X., and J. R. Key, 2005: Arctic surface, cloud, and radiation properties based on the AVHRR Polar Pathfinder Dataset. Part I: Spatial and temporal characteristics. *J. Climate*, 18, 2558–2574, doi:<https://doi.org/10.1175/JCLI3438.1>.
- Wendler, G., F. D. Eaton, and T. Ohtake, 1981: Multiple reflection effects on irradiance in the presence of Arctic stratus clouds. *J. Geophys. Res.*, 86, 2049–2057, doi:<https://doi.org/10.1029/JC086iC03p02049>.
- Whitaker, J. S., and T. M. Hamill, 2002: Ensemble data assimilation without perturbed observations. *Mon. Wea. Rev.*, 130, 1913–1924, doi:[https://doi.org/10.1175/1520-0493\(2002\)130<1913:EDAWPO>2.0.CO;2](https://doi.org/10.1175/1520-0493(2002)130<1913:EDAWPO>2.0.CO;2).
- Wu, X., and R. Grumbine, 2013: Sea ice in the NCEP Climate Forecast System Reanalysis. *Science and Technology Infusion Climate Bulletin, 38th NOAA Annual Climate Diagnostics and Prediction Workshop*, College Park, MD, NWS, 8 pp. [Available online at <http://www.nws.noaa.gov/ost/climate/STIP/38CDPW/38cdpw-XWu.pdf>.]
- Xi, B., X. Dong, P. Minnis, and M. M. Khaiyer, 2010: A 10 year climatology of cloud fraction and vertical distribution derived from both surface and GOES observations over the DOE ARM SPG site. *J. Geophys. Res.*, 115, D12124, doi:<https://doi.org/10.1029/2009JD012800>.

Xi, B., X. Dong, P. Minnis, M. M. Khaiyer, and S. Sun-Mack, 2014: Comparison of marine boundary layer cloud properties from CERES-MODIS edition 4 and DOE ARM AMF measurements at the Azores. *J. Geophys. Res. Atmos.*, 119, 9509–9529, doi:<https://doi.org/10.1002/2014JD021813>.

Xu, K.-M., and D. A. Randall, 1996: A semiempirical cloudiness parameterization for use in climate models. *J. Atmos. Sci.*, 53, 3084–3102, doi:[https://doi.org/10.1175/1520-0469\(1996\)053<3084:ASCPFU>2.0.CO;2](https://doi.org/10.1175/1520-0469(1996)053<3084:ASCPFU>2.0.CO;2).

Zib, B. J., X. Dong, B. Xi, and A. Kennedy, 2012: Evaluation and intercomparison of cloud fraction and radiative fluxes in recent reanalyses over the Arctic using BSRN surface observations. *J. Climate*, 25, 2291–2305, doi:<https://doi.org/10.1175/JCLI-D-11-00147.1>.